Verification of Block Kinematic Response as Calculated by ABAQUS DSO-98-009

Dam Safety Office

July 1999

Verification of Block Kinematic Response as Calculated by ABAQUS
DSO-98-009

by
Barbara L. Mills/Bria

U.S. Department of Interior
Bureau of Reclamation
Dam Safety Office

July 1999

BUREAU OF RECLAMATION
Technical Service Center, Denver, Colorado
Civil Engineering Services
Structural Analysis Group, D-8110

Dam Safety Research Report No. DSO-98-009

Verification of Block Kinematic Response as calculated by ABAQUS/Explicit

Prepared: _____
Barbara L. Mills/Bria

Checked: _____
Larry K. Nuss

Peer Review: _____
Gregg Scott (Technical Specialist)

Team Leader: _____ 7/12/99
Larry K. Nuss Date

Date	Description	Prepared	Checked	Peer Review	Team Leader

Introduction

The study of rigid body motion is important in the consideration of the behavior of dam under earthquake motion. Discrete blocks can be formed during the earthquake and the response of these blocks to subsequent earthquake motion is an important consideration. Research on the response of rigid bodies has been done since the late 1890's, although tools to predict the response of rigid bodies are scarce. The nonlinear capabilities of ABAQUS are studied here to understand how closely it can model the rigid body motion of a block compared to the theoretical solutions posed thus far.

Theory

A) Critical accelerations and friction factors

Consider a block of base width **B**, height **H**, weight **W**. (See Figure 1) Assume the coefficient of friction between the base and the supporting plane is **μ**. If a horizontal acceleration of $\mathbf{a}_y$ is applied to the supporting plane, overturning will occur when the moment of horizontal inertia about one edge is greater than the restoring moment due to the weight of the block.

$$\frac{W}{g}a_y\frac{H}{2}>W\frac{B}{2} \tag{1.1}$$

This implies that overturning will occur when:

$$a_y>\frac{B}{H}g \tag{1.2}$$

For this to be true the coefficient of friction must be great enough to ensure that the block won't slide. When

$$a_y\frac{W}{g}=\mu\frac{W}{g}g \tag{1.3}$$

or

$$\mu=\frac{a_y}{g} \tag{1.4}$$

the block just begins to slide. When

$$\mu > \frac{a_y}{g} \tag{1.5}$$

or:

$$\mu > \frac{B}{H} \tag{1.6}$$

the block will overturn before it slips.

B) Tall slender bodies

1) Constant acceleration

Housner developed the equations of motion for tall, slender structures in 1963 [1]. The equation of motion for a tall, slender block subjected to a constant horizontal acceleration of finite duration is found to be:

$$I_o \frac{d^2\theta}{dt^2} - mgr\theta = mgr\frac{a}{g} - mgr\alpha \tag{1.7}$$

where $\mathbf{I_o}$ = moment of inertia about the base edge of a body, θ = the angle through which the body has rotated, **m** = the mass of the block, **g**= acceleration due to gravity, **r** = the distance from the center of the block to the center of rotation, and α = the angle between the vertical edge of the block and the line from the center of the block to the center of rotation (see Figure 1).

For a tall, slender block, **B/H** approaches α, and the solution to this equation with initial condition equal to zero (ie $\theta = d\theta\ dt = 0$ at $t = 0$) is:

$$\frac{\theta}{\alpha} = \left(\frac{a}{g\alpha} - 1\right)(\mathbf{cosh}nt - 1) \tag{1.8}$$

where:

$$n = \sqrt{(mgr)/I_o}$$

As **B/H** approaches α, the limiting value for the acceleration amplitude before overturning

initiates becomes α*g. (See Eq. 1.2) If **a/g** is equal to α, the solution is zero, and the block will not overturn. If **a/g** > α, and if the acceleration acts for a sufficient time period, the block will overturn. For each value of **a** , there is a time t_0 , during which the acceleration can generate a velocity sufficient to overturn the block. Overturning will occur when the total work done by the inertia force, **ma**, is just equal to the difference in potential energy between positions $\theta = \alpha$ and $\theta = 0$. This leads to the solution:

$$\cosh nt_0 = 1 + \frac{1}{2\frac{a}{g\alpha}\left(\frac{a}{g\alpha} - 1\right)} \tag{1.9}$$

Figure 2 shows a plot of accelerations and the time period the acceleration must be applied to cause the block to tip. To obtain the plot shown in Figure 2, various values of **x = nt** were assumed and **y = cosh(nt)** was calculated. Given Eq. 1.9, the value of constant acceleration **a** can be calculated. Conversely, given a constant acceleration, **a**, the time **t=nt/n** in which a block will overturn is known. An acceleration **a > (B/H) g** , acting for the time period, **t**, will cause the block to overturn.

2) Sinusoidal acceleration

When the input motion is a sine wave, expressed by **a(t)= -a sin ((2π/T) t +** δ**)**, the relationship between the input motion and the characteristics of the block is:

$$\frac{a}{g\alpha} = \sqrt{1 + \frac{I_o}{mgr}\left[\frac{2\pi}{T}\right]^2} \tag{2.0}$$

where **a** is the amplitude of the sine wave and **T** is the period. This equation can be solved for various accelerations and half periods, just as was the case with Eq. 1.9. Figure 3 shows the input half sine wave and the relationship between the amplitude, **a**, and the period of the sine wave, **T**. Note that as **T** gets larger, the amplitude approaches the limiting value of **g***α. In the case of a sine wave, when the amplitude, **a** is greater than **g***α, as **a** increases, the half period, **t = T/2**, (the time in which tipping will be initiated), approaches zero and when **a** approaches **g***α, the half period, **t**, (the time in which tipping will be initiated) approaches infinity.

3) Earthquake acceleration

The response of a block to earthquake acceleration is similar to, but much more complicated than the response to either constant or a half pulse sine wave acceleration. It is possible that a series of pulses, even with accelerations less than **(B/H)*g** or α***g** could overturn a block or that a series of pulses with accelerations greater than **(B/H)*g** or α***g** could rock but not overturn given block. At best, probabilities of these events can be speculated upon. Housner [1] developed equations which help predict the behavior of a block based on it's size, **r** (see Figure 1) and the

velocity spectral intensity of the applied motion. These equations are restated in a study by Yim, Chopra and Penzien [2] in which the response of a rigid block was assessed using a computer code developed for their study. For a given pseudo spectral velocity, S_v, the equation describing a 50 percent probability of being overturned is:

$$\alpha = \frac{S_v}{\sqrt{gr}} * \sqrt{(mr^2)/I_o} \tag{2.1}$$

For rectangular blocks, $I_o = (m/3)\,(B^2 + H^2)$ and $r = (\frac{1}{2})\,(B^2 + H^2)$, so this becomes:

$$\alpha = 0.866 * \frac{S_v}{\sqrt{gr}} \tag{2.2}$$

For tall slender blocks, this equation approaches:

$$\alpha = \frac{S_v}{\sqrt{gr}} \tag{2.3}$$

The spectral velocity needed to overturn a block, increases with increasing size, as measured by **r**, for a constant ratio, **B/H** and increases with increasing slenderness ration **B/H**, for a constant **r**. This is shown in Figure 4. Recall that the block in question is a rigid block, so the fundamental period of the block is zero. Therefore, the spectral velocity discussed here is for a period of zero. The blocks modeled here using ABAQUS are not perfectly rigid but have relatively high fundamental frequencies (for block where B/H=1, the fundamental frequency is 512 Hertz, for the block where B/H=0.2, the fundamental frequency is 30.5 Hertz).

C) Block with ratio B/H = 1

Studies were undertaken using a deformable block with the dimensions **B=2** and **H=2.** The block was comprised of 8 deformable elements of type CPE4R: a reduced integration, 4-node plane strain element. This block rested on a two-dimensional, rigid surface (element type R2D2). The following values were assumed for this analysis: mass density of the block, $\delta = 10$, the stiffness of the block, $\mathbf{E}=1\text{x}10^9$, friction, $\boldsymbol{\mu}=2.0$. Damping was not included.

1) Constant acceleration

Gravity was ramped on in one second, followed by a constant acceleration applied to the base which was ramped on in 3 seconds and then held constant. Initially tests were run (on a block

with B/H = 0.2) to determined the effect of ramping on the acceleration vs, applying it all at once. Results of these tests showed that when the acceleration was applied instantaneously, accelerations and reactions forces spiked and then fluctuated in a diminishing manner about the values resulting from ramping on the acceleration. Displacements were not perceptively different and velocities converged quickly. (See Figure 5) This indicates that the acceleration should be ramped. In all subsequent runs, the constant acceleration was ramped on.

The rigid base on which the deformable block **(B/H = 1)** rested, was subjected to two different magnitudes of constant acceleration, from the left to the right. These included accelerations which were less than **(B/H)g** and greater than **(B/H)g** . The response of the deformable block was monitored. To determine if and when the block began to tip, the vertical acceleration and displacement of the lower left hand corner was considered, as well as the reaction forces at the five nodes along the base.

Figure 6 shows the results from the analysis in which the applied acceleration in the horizontal direction is less than **(B/H)g**. Figure 6a shows the applied horizontal acceleration and the vertical acceleration of the lower right-hand corner of the block. Note that the acceleration of the corner fluctuates around zero. The vertical and relative horizontal displacement of the lower right-hand corner is shown in Figure 6b. Note that the movement shown here is very small and is only the "chattering " of the corner against the rigid base as the acceleration is applied to the base. Figure 6c shows the variation in the reaction forces along the base. The leading three nodes are lifted off the rigid base, while the back two nodes continue to be in contact, to different degrees. Figure 6d shows the displaced shape of the block, magnified 3000 times, 2.75 seconds into the constant acceleration. As predicted by the above equations, the block does not tip.

Figure 7 shows the results when the constant horizontal acceleration is greater than **(B/H)g**. In this case the block is expected to tip. Figure 7a show the applied horizontal acceleration and the resulting vertical acceleration of the lower right-hand corner. Note that unlike the previous example, this time the resulting acceleration continues to increase beginning at 4.0 seconds, when the applied acceleration has first reached its maximum value. The movement of the lower right-hand corner is shown in Figure 7b. Note that the lower right hand corner is moving up and to the left as would be expected when the blocks tips. In Figure 7c it is seen that between 3.5 and 4.0 seconds the total reaction force is experienced by the lower left-hand corner of the block. Figure 7d shows the displacement of the block magnified 10 times, at the time when the acceleration has first reached is maximum value. The block has begun to tip.

2) Sinusoidal acceleration

Next, this block was subjected to two sine wave accelerations, one in which the amplitude was less than **(B/H)g** and one in which the amplitude was greater than **(B/H)g**. The results of the first analysis are shown in Figure 8. It is clear from this figure that the block does not tip, although the contact between the base of the block and the rigid surface "chatters".

Finally, the block was subjected to a sine wave acceleration in which the amplitude was greater than **(B/H)g**. The results of this analysis are shown in Figure 9. A comparison of the input

horizontal acceleration and the resulting vertical acceleration of the lower right-hand corner is shown in Figure 9a. Figure 9b compares the input acceleration with the lateral movement and vertical movement of the lower right-hand corner and of the block. As would be expected the reaction force at the lower right hand corner diminishes to zero and the reaction force at the lower left hand corner increases. As seen in Figure 9d, the block has begun to tip.

D) Block with ratio B/H = 0.2

This block was modeled as a deformable body, consisting of forty elements of type CPE4R: a reduced integration, 4-node plane strain element. (See Figure 10) This block rests on a two-dimensional, rigid surface (element type R2D2). The following values were assumed for this analysis: mass density of the block, $\delta = 10$, the stiffness of the block, $E = 1 \times 10^9$, gravity, $g = 100$. The coefficient of friction, μ, was assumed to be 0.6 which is greater than **B/H**.

1) Constant acceleration

The first analysis was done using an acceleration equal to 19, which was less than **(B/H)*g**. Gravity was ramped on in one second, followed by a constant acceleration applied to the base which was ramped on in one second and then held constant. As was true with the previous model, the acceleration of the rigid base was left to right, so if the model were to pivot, it would be about it's lower left-hand corner. Therefore, overturning was monitored by checking the vertical displacement and acceleration of the lower right-hand corner of the model, the horizontal displacement of the lower right-hand corner and the reaction forces at the lower left-hand corner of the model. The results of this analysis are shown in Figure 10. The block wobbled but did not overturn. The chattering of the lower right hand corner of the model can be seen in Figure 10b. Notice in Figure 10a that the acceleration oscillates around zero and in Figure 10b that the vertical displacement of this corner oscillates about 0.6×10^{-3} . As the rigid base is accelerated to the right, the leading corner vibrates, but the block remains upright.

Next the acceleration applied to the rigid base was increased to 21.94, which is greater than **(B/H)* g**. According to Eq. 1.9, the block should overturn in 0.6 seconds. The block begins to tip and after 0.8 seconds (this is equivalent to 3.8 seconds in the plot), the block has reached the point where it will continue to overturn. Figure 11a and 11b show the increasing vertical acceleration and the increasing vertical and horizontal displacement of the lower right-hand corner of the model Note that as seen in Figure 11c, as the block rotates around that corner, the reaction force at the lower left-hand corner increases to 20000, the weight of the block, and then begins to diminish as the block continues to overturn. Figure 11d shows the position of the block 0.8 seconds after the acceleration of the rigid base has reached it's maximum value.

2) Sinusoidal acceleration

The same model was then subjected to various sine wave half pulse accelerations. First a value of acceleration amplitude, **a** less than α***g** was selected. The half period, **t** was chosen to be very high. Recall that when the acceleration amplitude, **a** is less than α***g**, there is no solution. However, as **a** greater than α***g**, approaches α***g**, the half period, **t** necessary to initiate tipping,

gets very large. The results of the $\mathbf{a} < \alpha^*\mathbf{g}$ analysis are shown in Figure 12. A comparison of the applied acceleration and the vertical acceleration of the lower-right hand corner of the model (Figure 12a) shows that the corner accelerates up and down, oscillating about zero. As can be seen, the lower right-hand corner of the model raises up off the rigid base very slightly, but no tipping is initiated. The plot of the reaction forces along the base also indicates this and shows that the three leading nodes of the base lift off the rigid base for a short while.

Next an acceleration amplitude slightly greater than $\alpha^*\mathbf{g}$ was applied to the model. The sine wave half pulse was determined for this amplitude to be 2. The results of this analysis are shown in Figure 13. The first plot shows a comparison of the applied acceleration and the vertical acceleration of the lower right-hand corner of the model. The acceleration of that corner increases to a maximum and then begins to decline. Figure 13b shows that the lower right hand corner lifts off the base as the block tips and then comes back down. This is also shown in the plot of reaction forces. In this case the block begins to tip, but does not overturn.

Finally, a half pulse sine wave with amplitude much greater than $\alpha^*\mathbf{g}$ was applied to the model. As is expected, the half period is very short (t = 0.3). However, the behavior of the block is similar to that of the previous example. (See Figure 14)

3) Earthquake acceleration

The tall, slender block used in the previous analyses was next subjected to time history earthquake motions. Based on Eq 2.2 the spectral velocity necessary to indicate a 50% chance of overturning for this block was S_v= 5.136. In order to simplify calculations , the acceleration due to gravity, **g**, was assumed to 100. The program RESPONS, modified to correct the value of **g** to 100, as used in this study, was used to determine the spectral velocity for the earthquake chosen for this analysis. The first 5 seconds of the Pleasant Valley Pumping record, with a peak g of 0.34 was used. The record was recorded updip of the fault rupture of the 1983 M 6.5 Coalinga blind thrust earthquake in the switchyard of Reclamation's Pleasant Valley Pumping Plant. The acceleration record was integrated to determine the velocity record. The block is very stiff, having a fundamental frequency of 30.5 Hertz. Because the block was very stiff, the value of the spectral velocity was assumed to be the maximum value of the velocity time history. It is possible to increase the spectral velocity of the record by multiplying the amplitude of the acceleration record, and therefore, also the velocity record, by a constant. The peak velocity for the record (using a value of g=100) was v=1.63. This is equal to 31.7 percent of S_v . Therefore, three analyses were run: the first using the acceleration record as is; the second using the acceleration multiplied by 3, resulting is a value of v = 4.89 or 95.2 percent of S_v ; and the third using the acceleration multiplied by 5, resulting in a value of v = 8.15 or 158 percent of S_v. The response of the block to these three variations of the acceleration record were studied. Figure 15 contains plots of the original acceleration and velocity records, the original acceleration and velocity records multiplied by 3 and the original acceleration and velocity records multiplied by 5. The velocity response spectra for these three cases is also plotted.

In the first case, where the maximum velocity was 31.7 percent of S_v, the block began to rock but did not overturn. The results of this analysis are shown in Figure 16. A comparison of the

vertical displacement of the lower right hand corner and the lower left hand corner is shown in Figure 16b. This shows that the block is rocking back and forth. Figures 16c and d show the block as it rocks to the left and back to the right for the last time. Figure 16e compares the vertical accelerations of the corners with the input acceleration. Figure 16f is a plot of the horizontal and vertical displacements of one corner. It shows that the corner lifts off the rigid support, but does not move horizontally with respect to the base. Figure 16 g compares the vertical velocities of the two lower corners and figure 16h shows the vertical reactions at the corners as the block rock back and forth.

When the spectral velocity was increased to 95.2 percent of S_v, the block rocked back and forth only three time before it overturned, 3.97 seconds into the acceleration record. Figure 17 b show the vertical displacements of the two lower corners as they alternate lifting off the rigid support. Figure 17 c and d show the block as it rocks to the right for the last time and then tips over to the left. shows Figure 17e compares the accelerations of the two lower corners and figure 17f compares the vertical and horizontal displacement of one lower corner. The vertical velocities of the two lower corners are compared in figure 17g and the reaction forces at the corners are compared in figure 17h. Note that following the overturning of the block, reactions at these two locations are zero.

Finally, the spectral velocity was increased to 158 percent of S_v. For this analysis, the block rocked twice before it overturned, 2.94 seconds into the acceleration record. Figure 18 b show the vertical displacements of the two lower corners as they alternate lifting off the rigid support. Figure 18 c and d show the block as it rocks to the right for the last time and then tips over to the left. shows Figure 18e compares the accelerations of the two lower corners and figure 18f compares the vertical and horizontal displacement of one lower corner. The vertical velocities of the two lower corners are compared in figure 18g and the reaction forces at the corners are compared in figure 18h. Note reactions at these two locations are zero following the overturning of the block.

E) Hoover model

Non-linear dynamic cracking analyses showed that with normal reservoir elevations an independent block could form at the top of Hoover Dam during earthquake excitation.[3]. A two dimensional model of this block was created using plane strain elements. It should be noted that arch action was not modeled in this study. As the dam experiences the earthquake motion, the contraction joints open and close. When the joints are closed, the block would be under compressive loads and movement would be restricted. In addition, friction forces along the sides of the block have also been ignored for this study. Therefore, movement here is much greater than that which would be expected in a three dimensional analysis which considered arch action and friction on the sides of the block.

Time varying accelerations, taken from the response of the dam at the base of the block, as determined by EACD3D [4] were applied to the rigid base on which the model rested. These accelerations and the corresponding velocities are shown in Figure 19. Also shown in this figure is the velocity response spectrum for this motion. Laboratory tests found that an apparent

cohesion value of 91 lb/in^2 and a friction angle of 47 degrees were appropriate for the concrete at Hoover Dam. The ABAQUS friction model uses only the friction angle and does not consider cohesion. For this model a friction coefficient of 1.1 was applied to the surface between the rigid base and the block. ABAQUS calculated the mass moment of inertia about the centroid for this two dimensional model to be 1.128 E+08. The mass of the block was 331.5 pound-second^2 / inch. For this analysis the concrete material properties were modulus of elasticity, E = 3.0 x 10^{6}lb/in^2 and a density of 150 lb/ft^3. The model is shown in figure 20.

The fundamental frequency of the block was 6.20 cycles/second and so the fundamental period is 0.16 seconds. This block is much less stiff than the rectangular block discussed previously. Figure 21 shows the fundamental mode shape.

In order to determine α, it was assumed that the edges of the block were vertical. Then the angle, α_1, for the left-hand side of the model is 28.4 degrees or 0.496 radians. This satisfies the "tall, narrow" block criteria since sin (28.4) = 0.476 $\approx$ 0.496. The value of r_1 is 962.8 inches. (See figure 20) Using these values in Eq 2.1, the spectral velocity which will imply a 50 percent chance of overturning is 9.44. Similarly, for the lower right-hand corner, the angle, α_2, is 12.9 degrees or 0.2245 radians. This also satisfies the "tall, narrow" block criteria since sin (12.9) = 0.223 $\approx$ 0.2245. The value of r_2 is 868.5 inches. (See figure 20) Using these values in Eq 2.1, the spectral velocity which will imply a 50 percent chance of overturning is 4.80. From Figure 19, one sees that the spectral velocity at a period of 0.16 seconds is around 12.0 in/sec. This is greater than either of the critical spectral velocities computed above, which implies that the chance of overturning is high. However, this neglects reservoir loading on the block.

For the analysis, all of the loads acting on the block were included. Hydrostatic and hydrodynamic pressure were input as pressure loads and vertical accelerations were included. These loads are shown in Figure 19 with the time history velocity records and the velocity response spectra. The behavior of the block is stable (see figure 22). The block moves to the left (red line on Figure 22b) while the lower right hand corner bounces (green line, Figure 22b). The lower left and lower right corners move up and down together, with the block tipped slightly upstream and with the lower left corner bearing all the weight (see Figures 22g and 22h). The block does not overturn.

Conclusions

ABAQUS/Explicit models the theoretical solutions for simple two-dimensional rectangular rigid blocks very well. Predictions for the outcome of each analysis based on theoretical solutions were achieved for constant, sinusoidal and earthquake accelerations. Even with a more complicated and less rigid block, the response of the block appears to be within reasonable limits. The extrapolation to three dimensions is less clear, however a two-dimensional analysis can be used to "check" the results of a three dimensional study.

References

1. Housner, G. W., "Behavior of Inverted Pendulum Structures during Earthquakes," Bulletin of the Seismological Society of America , Vol. 53, No.2, pp. 404-417, 1963.

2. Yim, C. S., Chopra, A. K, Penzien, J., "Rocking Response of Rigid Blocks to Earthquakes," Report # UCB/EERC-80/02, College of Engineering, University of California- Berkely,CA, Jan. 1980.

3. Koltuniuk, Roman M., "Nonlinear Dynamic Structural Analysis of Hoover Dam Including Modeling of Contraction Joints and Concrete Cracking ", Bureau of Reclamation, Technical memorandum number HVD-8110-MDA-97-4, September 1997.

4. Payne, T.L., "Effects of Water Compressibility on Dynamic Structural Analysis for Hoover Dam, Bureau of Reclamation", Technical memorandum number HVD-MDA-D8110-97-3, September 1997.

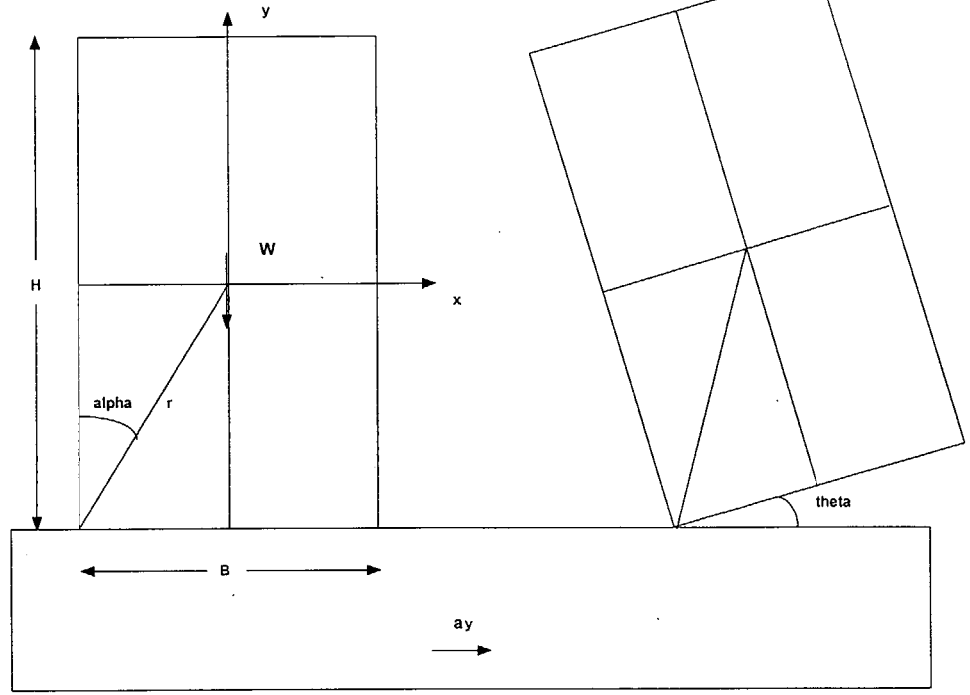

Motion of a Rectangular block

Figure 1

volume=	20
mass density=	10
alpha=	0.197396
g=	100
m=mass density*vol	200
r=	5.09902
Io=m{b**2/12 + h**2/3)	6733.333
b=	2
h=	10
n = sqrt (mgr/Io)	3.891735

$$\cosh(nt) = \frac{1}{2 * a/(g*\alpha)[a/(g*\alpha) - 1]}$$

x=nt	y=cosh(nt)	t=x/n	a(y)
1	1.5431	0.2570	31.227518
1.1	1.6685	0.2827	29.588818
1.2	1.8107	0.3083	28.247557
1.3	1.9709	0.3340	27.134596
1.4	2.1509	0.3597	26.200526
1.5	2.3524	0.3854	25.409090
1.6	2.5775	0.4111	24.733078
1.7	2.8283	0.4368	24.151668
1.8	3.1075	0.4625	23.648652
1.9	3.4177	0.4882	23.211227
2	3.7622	0.5139	22.829145
2.1	4.1443	0.5396	22.494104
2.2	4.5679	0.5653	22.199310
2.3	5.0372	0.5910	21.939150
2.4	5.5569	0.6167	21.708947
2.5	6.1323	0.6424	21.504775
2.6	6.7690	0.6681	21.323315
2.7	7.4735	0.6938	21.161742
2.8	8.2527	0.7195	21.017640

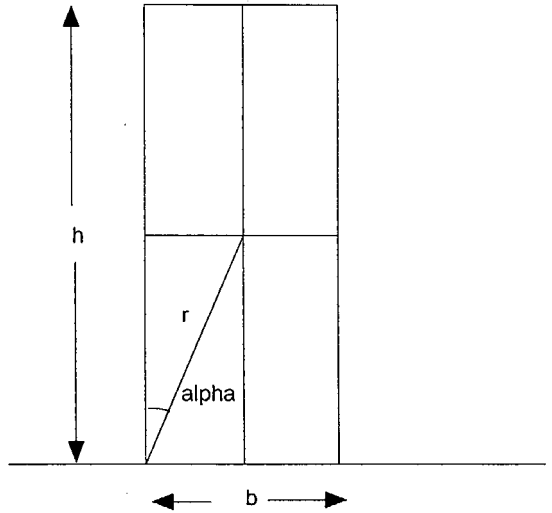

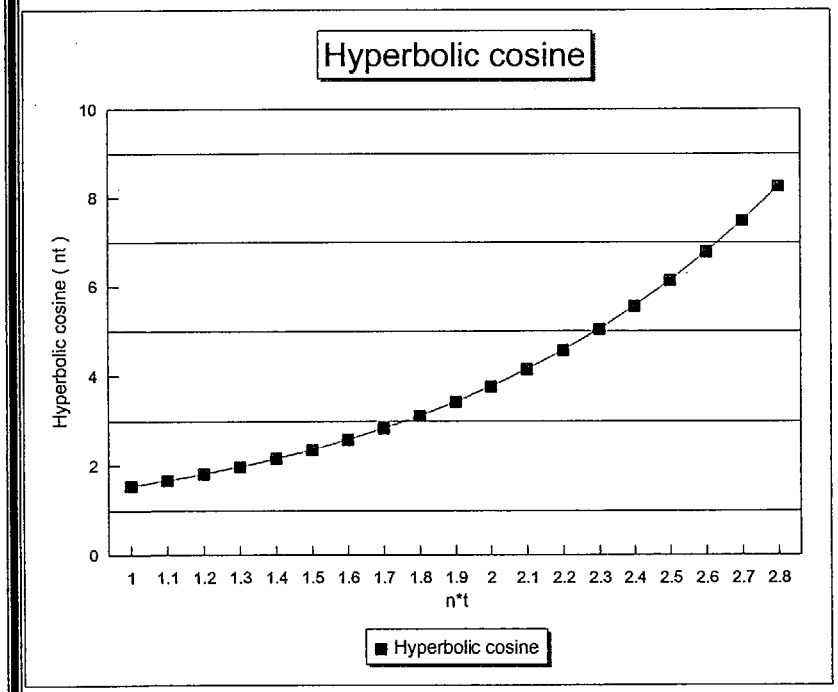

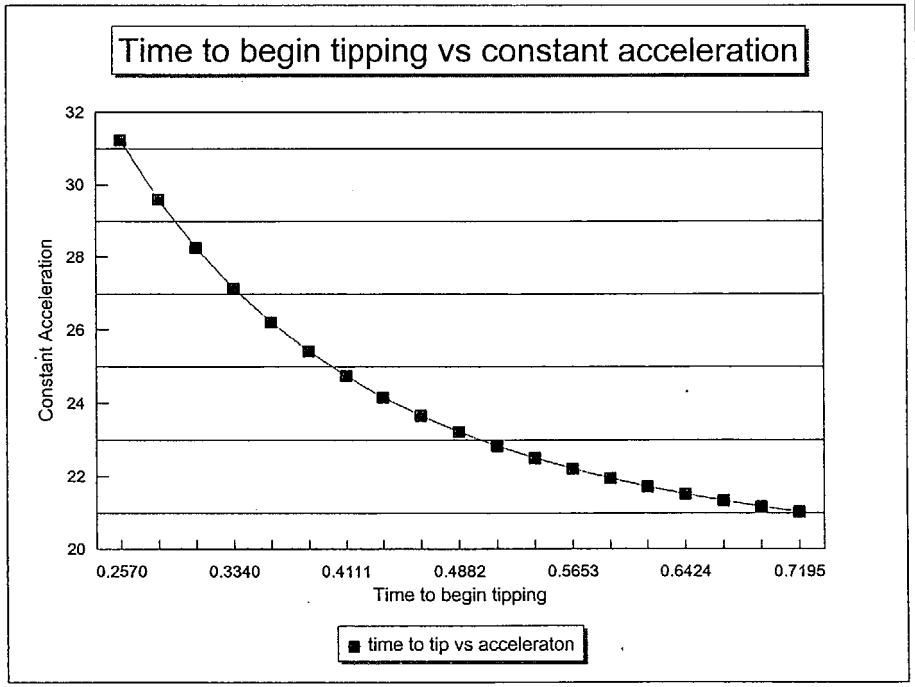

Figure 2

volume=	20
mass density=	10
alpha=	0.197396
g=	10
m=mass density*vol	200
r=	5.09902
Io=m{b**2/12 + h**2/3)	6733.333
b=	2
h=	10
n = sqrt (mgr/Io)	1.230675

$$\cosh(nt) = \frac{1}{2 * a/(g*\text{alpha})[a/(g*\text{alpha}) - 1}$$

x=nt	y=cosh(nt)	t=x/n	a(y)
1	1.5431	0.8126	3.122752
1.1	1.6685	0.8938	2.958882
1.2	1.8107	0.9751	2.824756
1.3	1.9709	1.0563	2.713460
1.4	2.1509	1.1376	2.620053
1.5	2.3524	1.2188	2.540909
1.6	2.5775	1.3001	2.473308
1.7	2.8283	1.3814	2.415167
1.8	3.1075	1.4626	2.364865
1.9	3.4177	1.5439	2.321123
2	3.7622	1.6251	2.282914
2.1	4.1443	1.7064	2.249410
2.2	4.5679	1.7876	2.219931
2.3	5.0372	1.8689	2.193915
2.4	5.5569	1.9501	2.170895
2.5	6.1323	2.0314	2.150478
2.6	6.7690	2.1127	2.132331
2.7	7.4735	2.1939	2.116174
2.8	8.2527	2.2752	2.101764

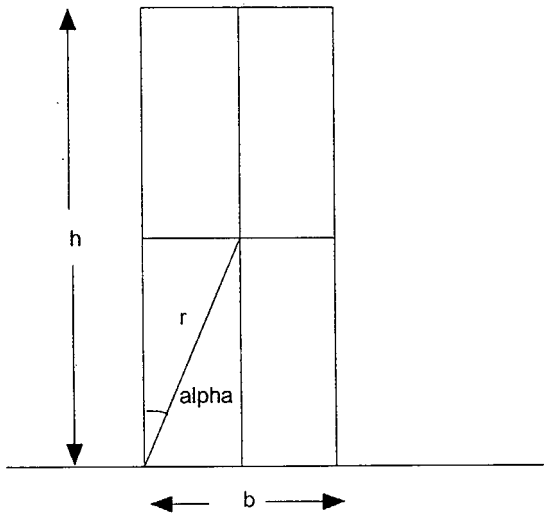

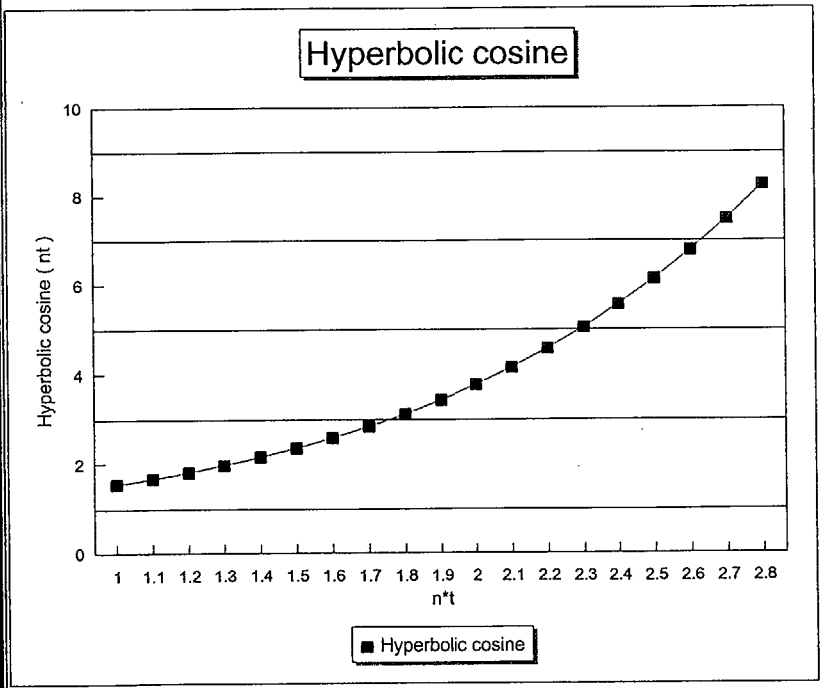

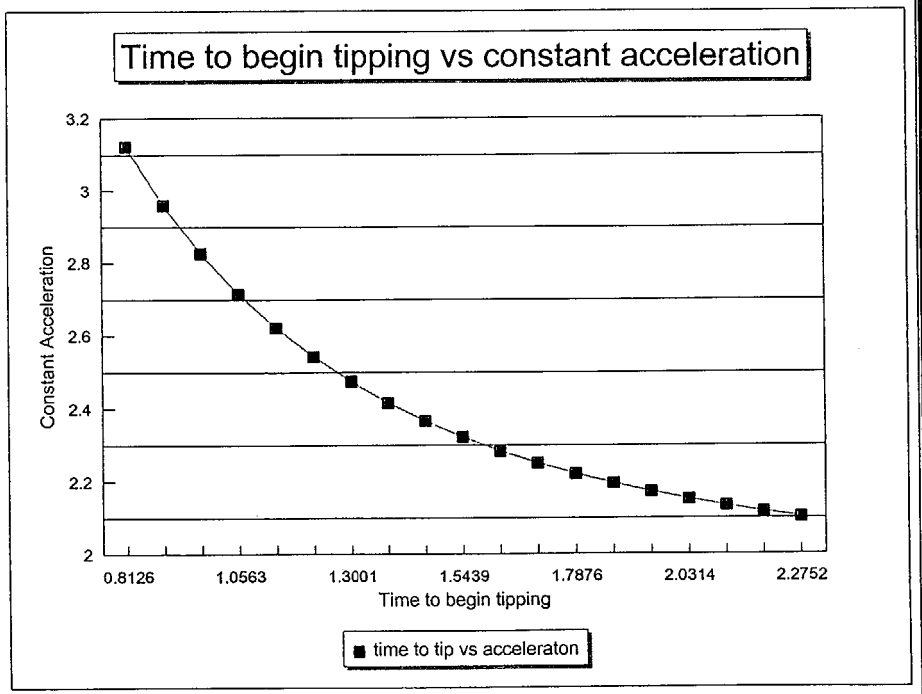

Figure 2

phase angel, delta=	0		Given period, T
period, T=	4		Calculate p/n = (2*pi/T)/n
p = 2*pi/T =	1.570796		Knowing p/n
volume=	20		Calculate a/(g * alpha) = Sqrt{1+(p/n)**2}
mass density=	10		Knowing g, alpha
alpha=	0.197396		Calculate acceleration amplitude, a
g=	100		
m=mass density*vol	200		
r=	5.09902		
Io=m{b**2/12 + h**2/3)	6733.333	6933.333	
b=	2		
h=	10		
n = sqrt (mgr/Io)	3.891735		
p/n =	0.403624		
acceleration amplitude =	4		

$$\frac{a}{g * alpha} = Sqrt\,[\,1 + \{\,Io/(mgr)\}\,\{2*\,pi/T\}\text{^}2]$$

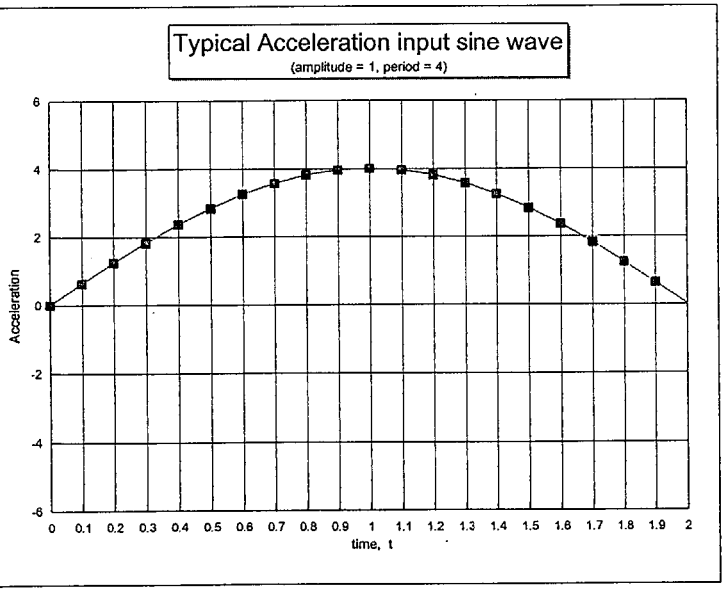

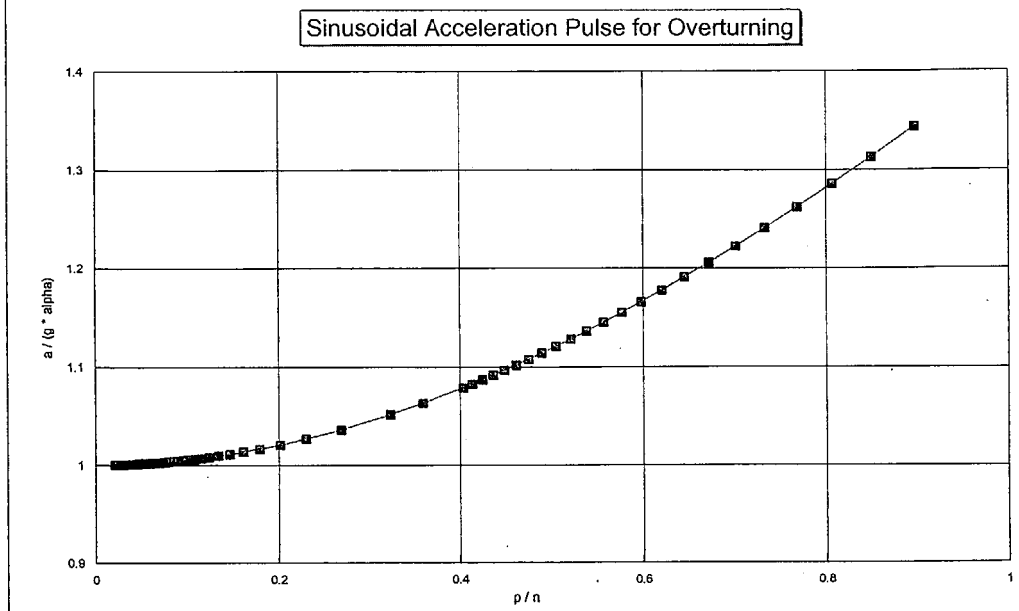

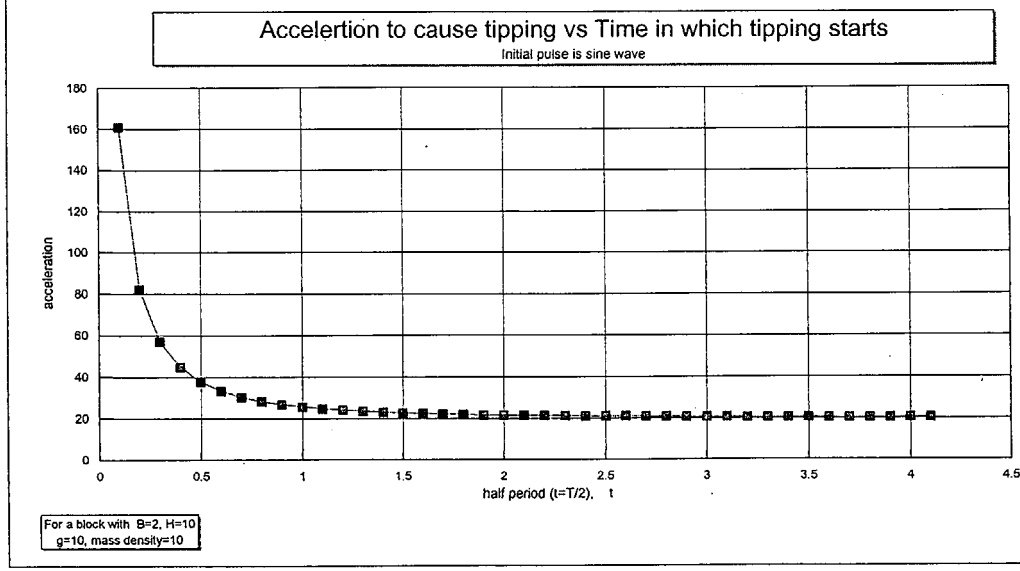

Figure 3

Spectral Velocity to Overturn (50 % chance)

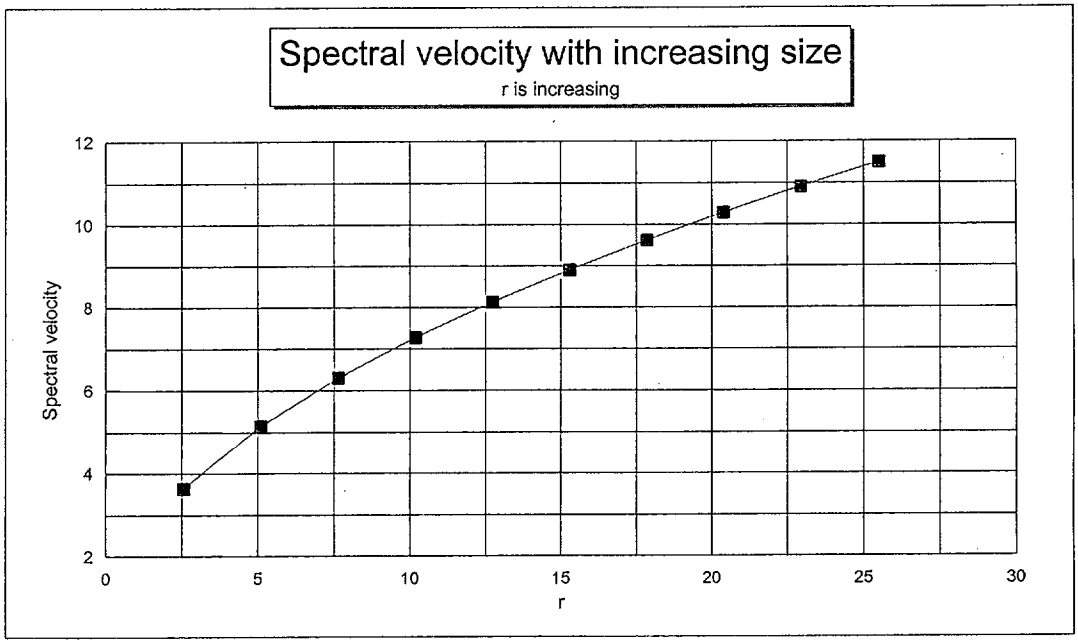

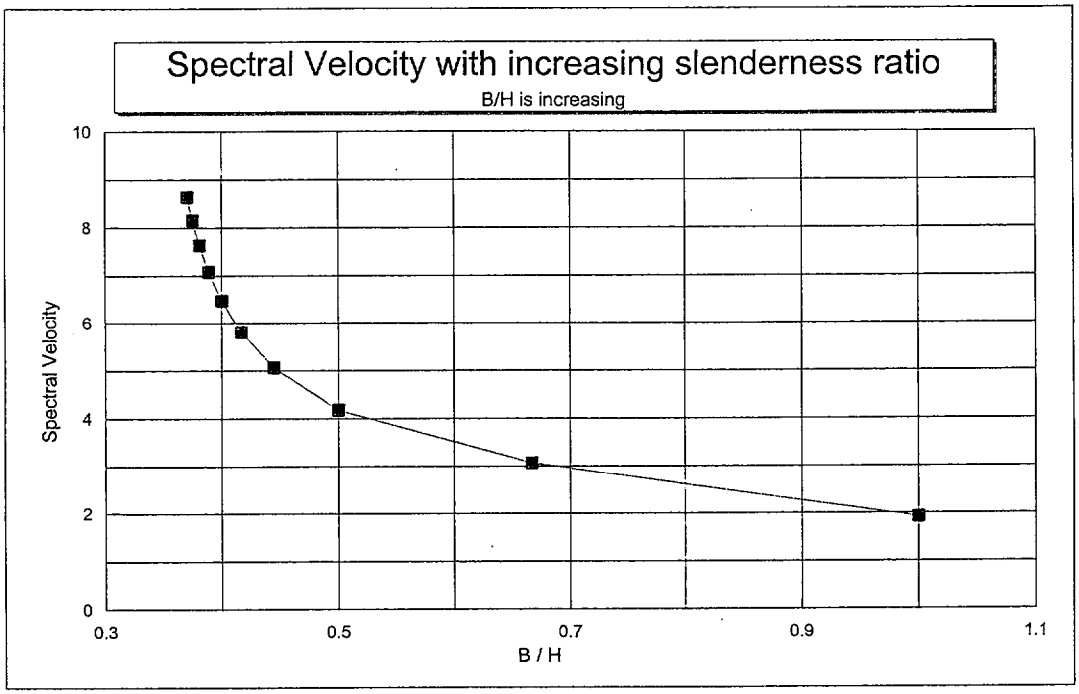

Angle alpha = 0.866 * Spectral Velocity / Square root (g * r)

Figure 4

ABAQUS

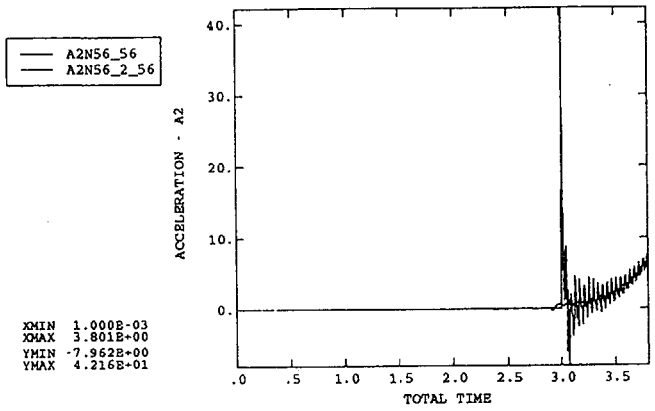

Acceleration of corner node

ABAQUS

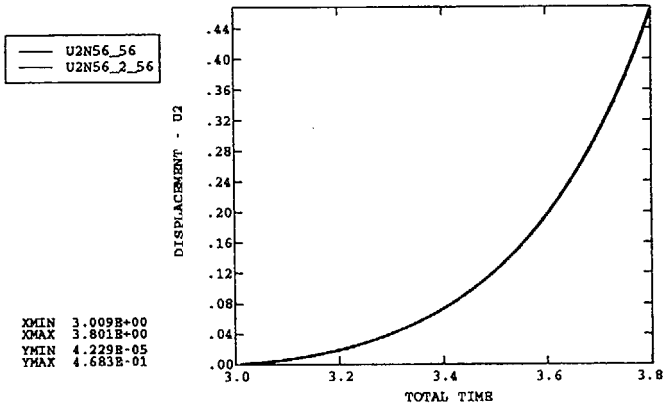

Displacement of corner node

ABAQUS

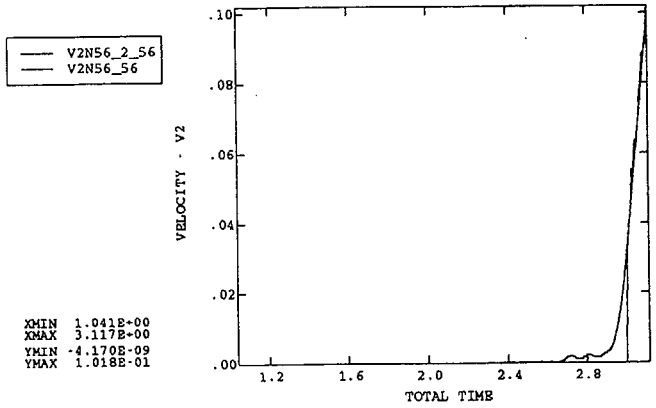

Velocity of corner node

ABAQUS

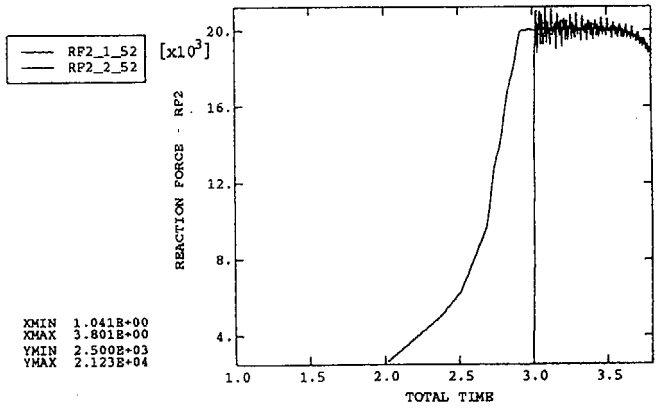

Reaction force at corner node

Figure 5

ABAQUS

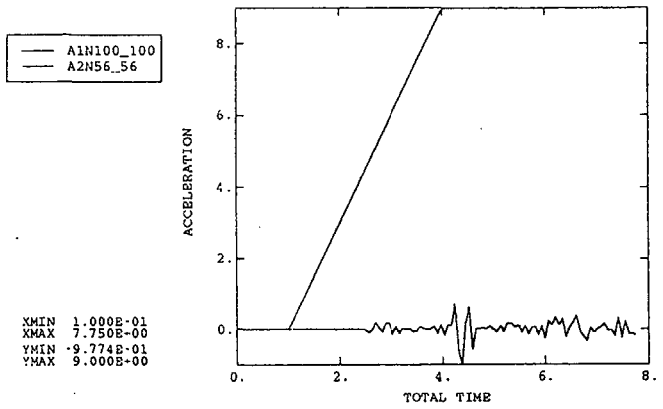

Figure 6a Applied horizontal acceleration
Vertical acceleration of corner

ABAQUS

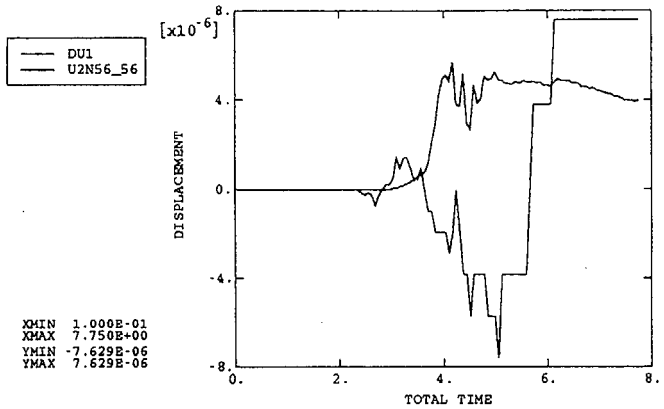

Figure 6b Vertical and horizontal
Displacement of corner

ABAQUS

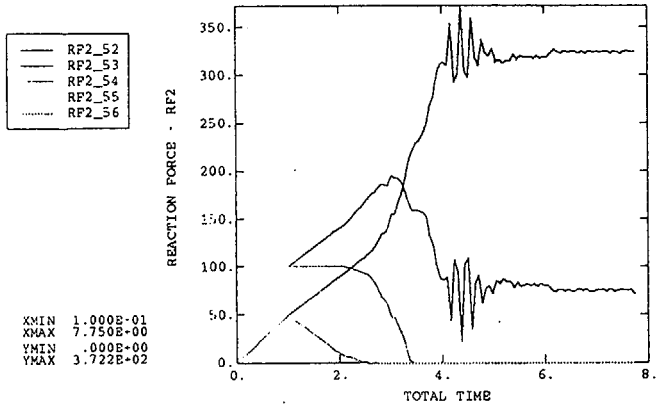

Figure 6c Reaction forces along base

ABAQUS

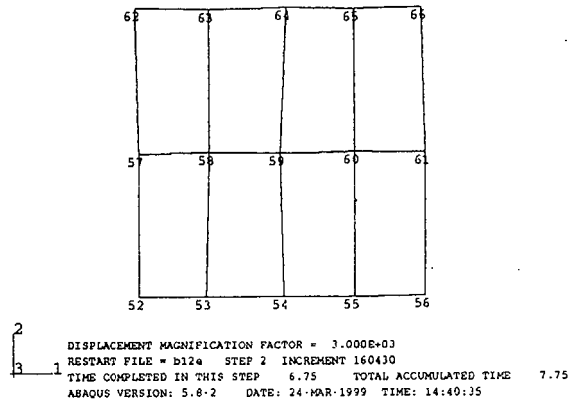

Figure 6d Displaced Block

Figure 6

ABAQUS

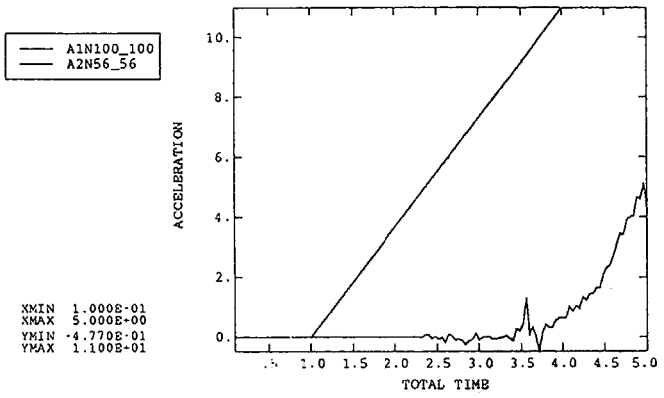

Figure 7a Applied horizontal acceleration
Vertical acceleration of corner

ABAQUS

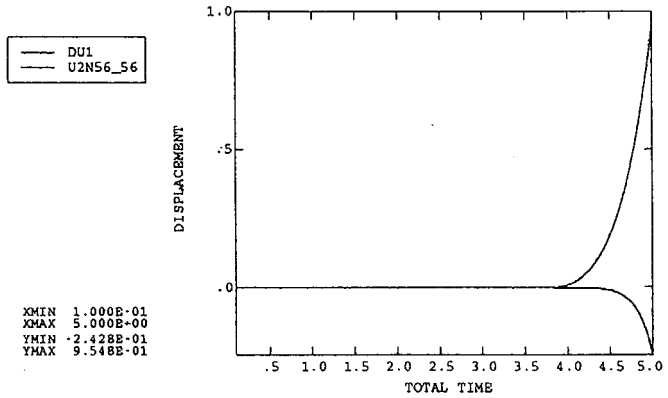

Figure 7b Vertical and horizontal
Displacement of corner

ABAQUS

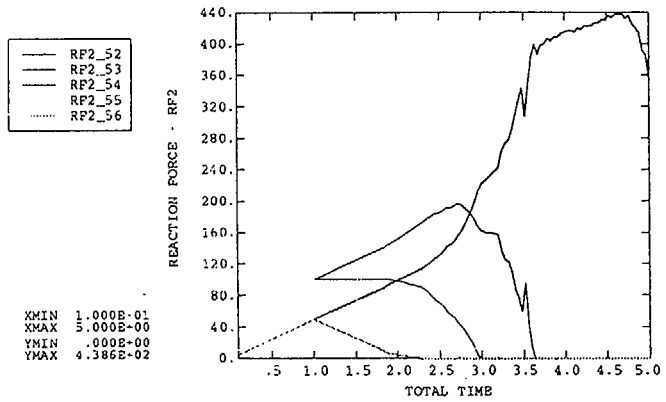

Figure 7c Reaction forces along base

ABAQUS

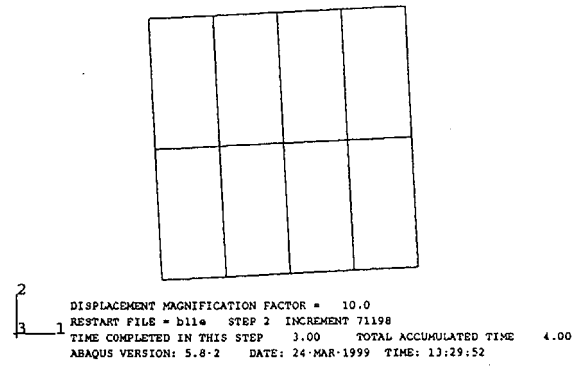

Figure 7d Displaced Block

Figure 7

ABAQUS

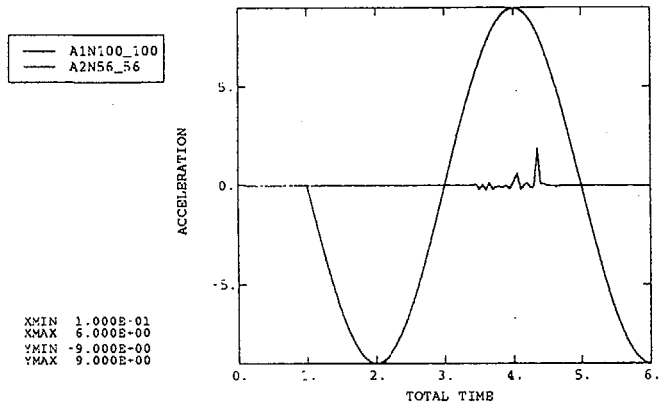

Figure 8a Applied horizontal acceleration
Vertical acceleration of corner

ABAQUS

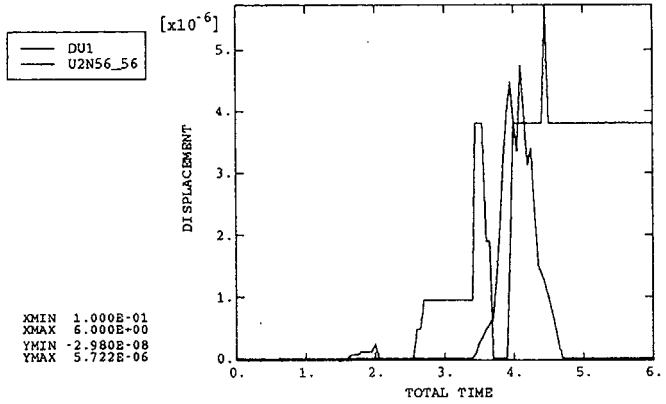

Figure 8b Vertical and horizontal
Displacement of corner

ABAQUS

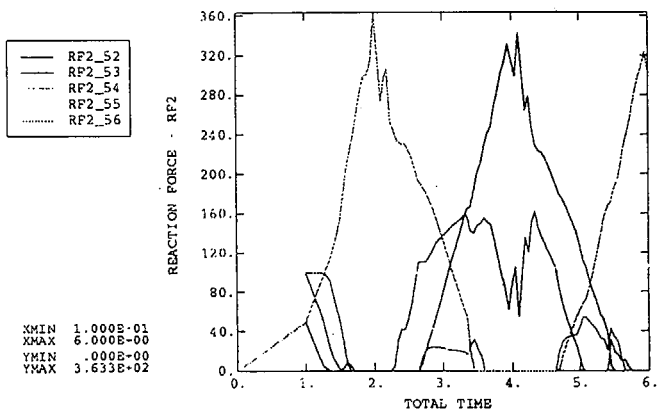

Figure 8c Reaction forces along base

ABAQUS

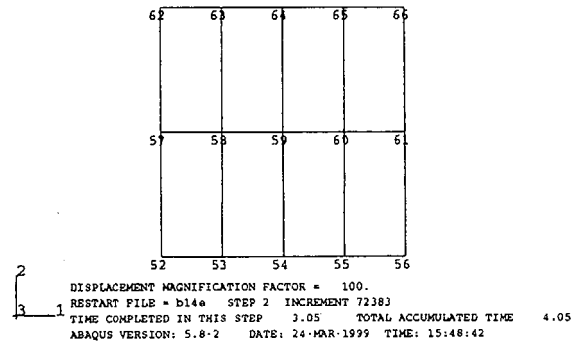

Figure 8d Displaced Block

Figure 8

ABAQUS

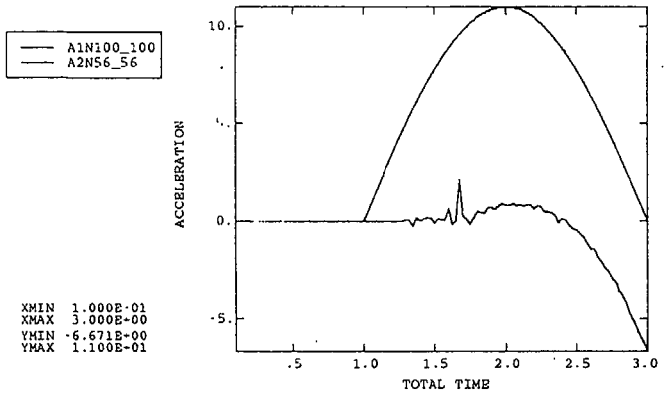

Figure 9a Applied horizontal acceleration
Vertical acceleration of corner

ABAQUS

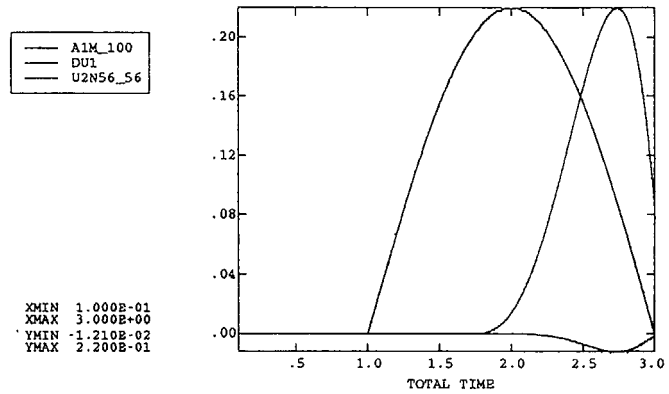

Figure 9b Vertical and horizontal
Displacement of corner

ABAQUS

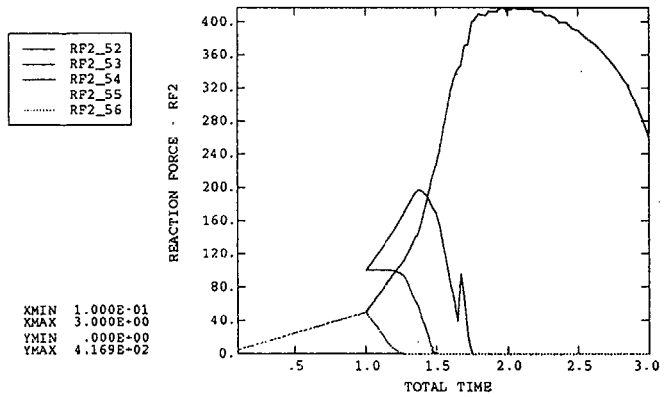

Figure 9c Reaction forces along base

ABAQUS

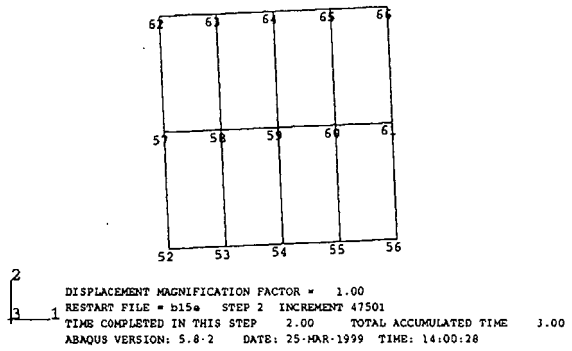

Figure 9d Displaced Block

Figure 9

ABAQUS

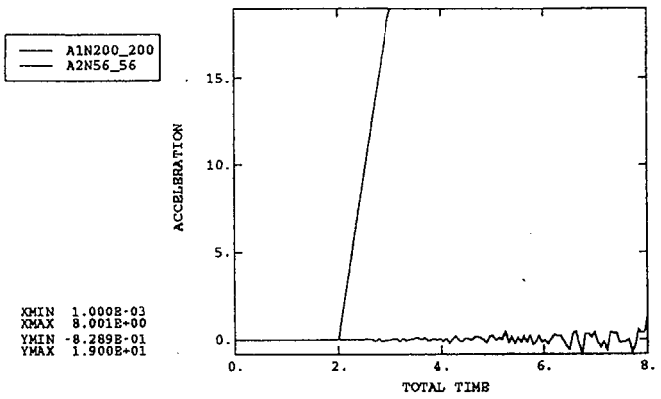

Figure 10a Applied horizontal acceleration
Vertical acceleration of corner

ABAQUS

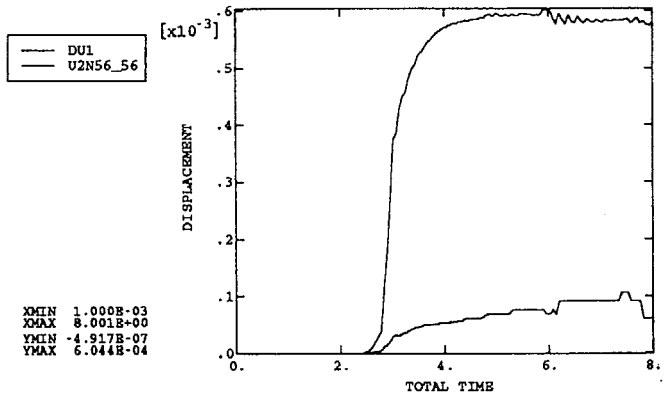

Figure 10b Vertical and horizontal
Displacement of corner

ABAQUS

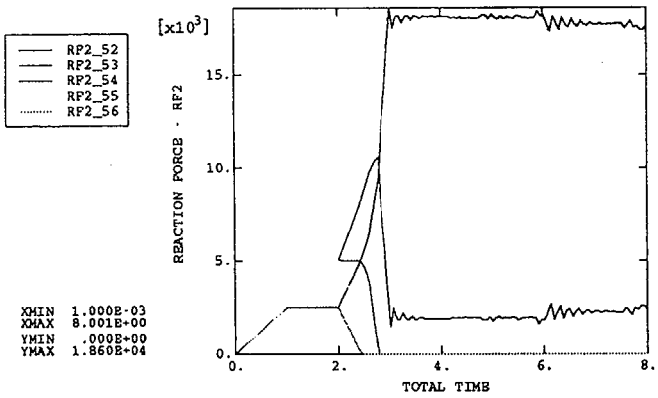

Figure 10c Reaction forces along base

ABAQUS

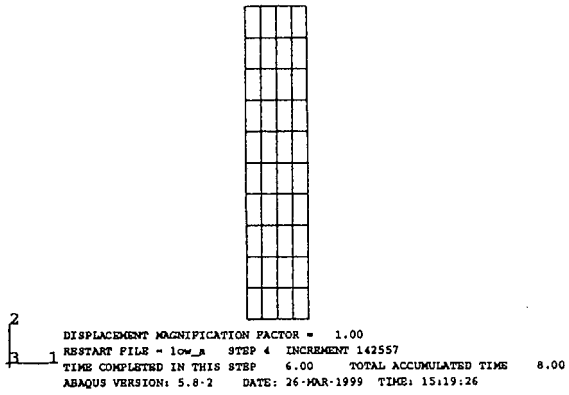

Figure 10d Displaced Block

Figure 10

ABAQUS

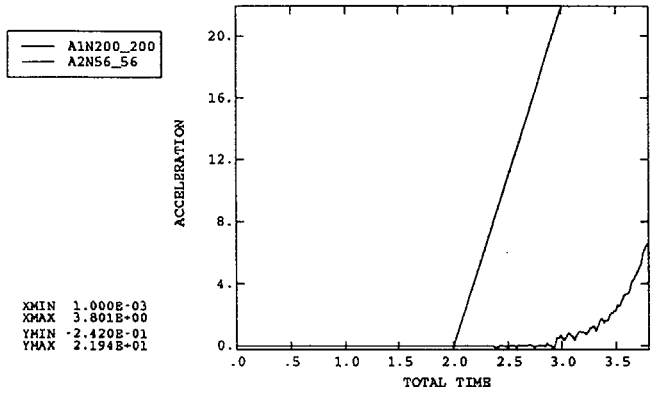

Figure 11a Applied horizontal acceleration
Vertical acceleration of corner

ABAQUS

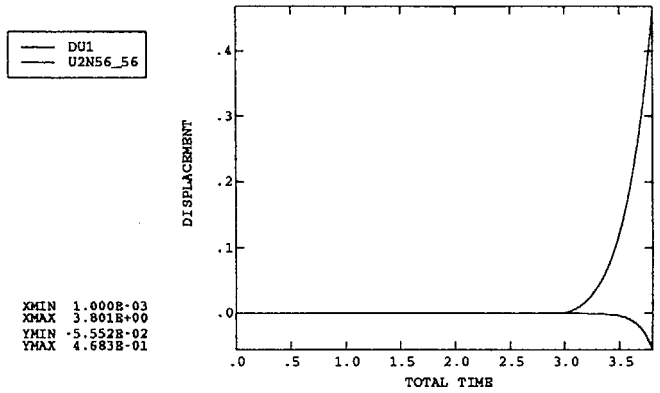

Figure 11b Vertical and horizontal
Displacement of corner

ABAQUS

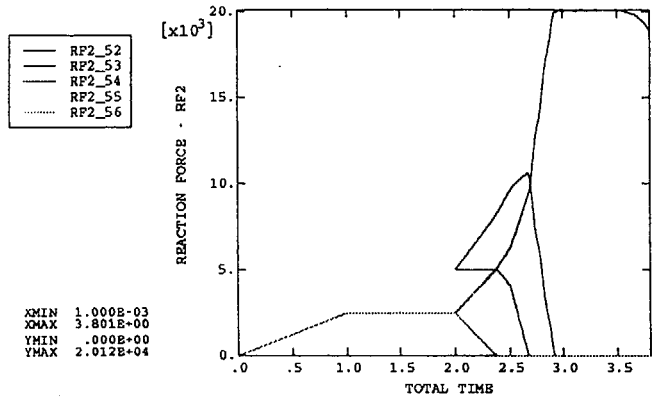

Figure 11c Reaction forces along base

ABAQUS

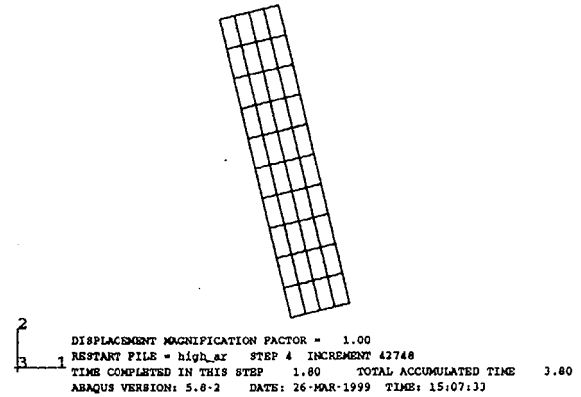

Figure 11d Displaced Block

Figure 11

ABAQUS

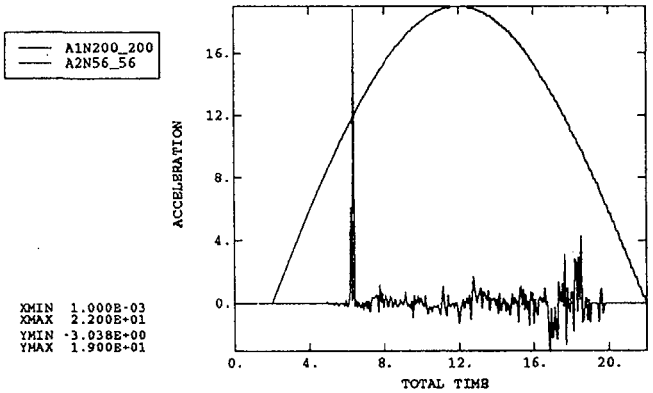

Figure 12a Applied horizontal acceleration
Vertical acceleration of corner

ABAQUS

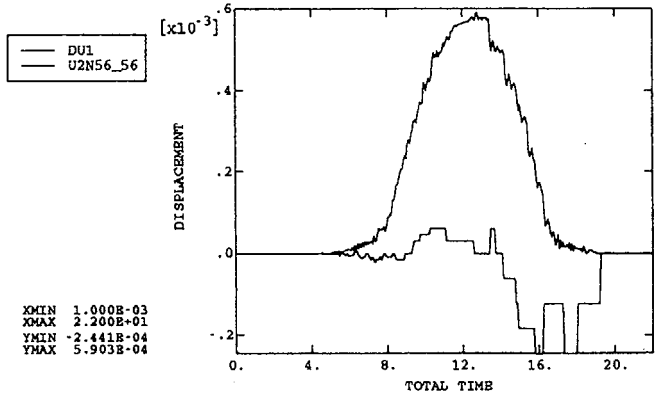

Figure 12b Vertical and horizontal
Displacement of corner

ABAQUS

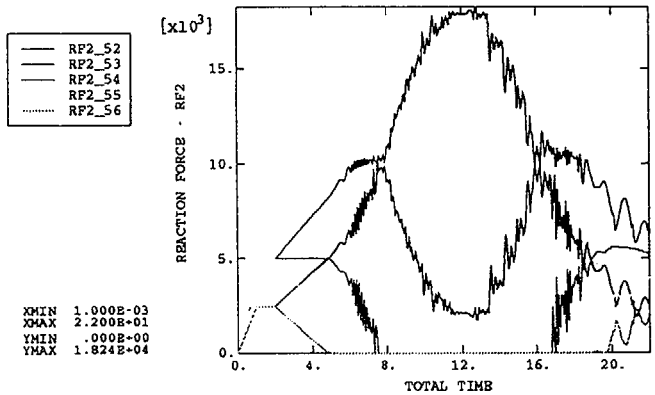

Figure 12c Reaction forces along base

ABAQUS

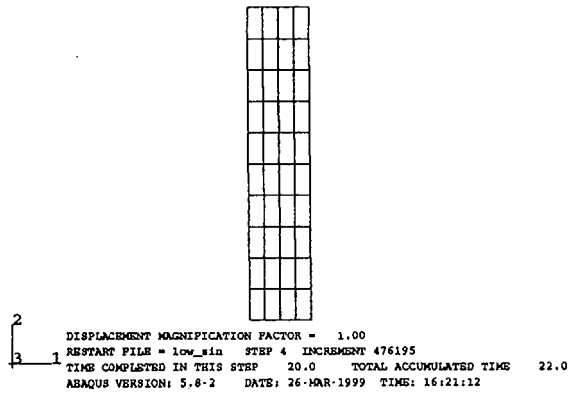

Figure 12d Displaced Block

Figure 12

ABAQUS

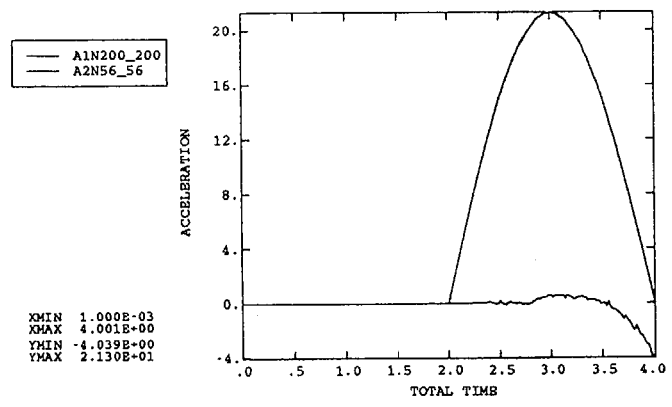

Figure 13a Applied horizontal acceleration
Vertical acceleration of corner

ABAQUS

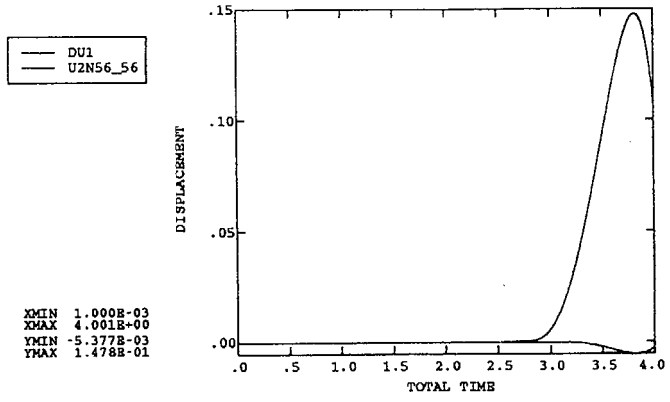

Figure 13b Vertical and horizontal
Displacement of corner

ABAQUS

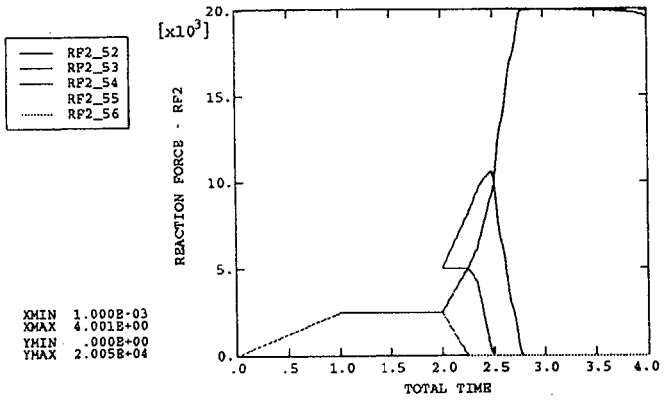

Figure 13c Reaction forces along base

ABAQUS

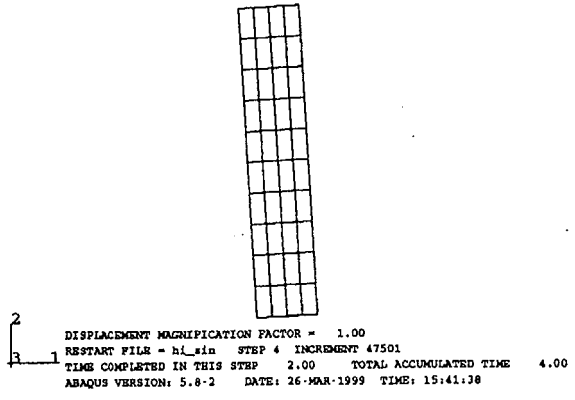

Figure 13d Displaced Block

Figure 13

ABAQUS

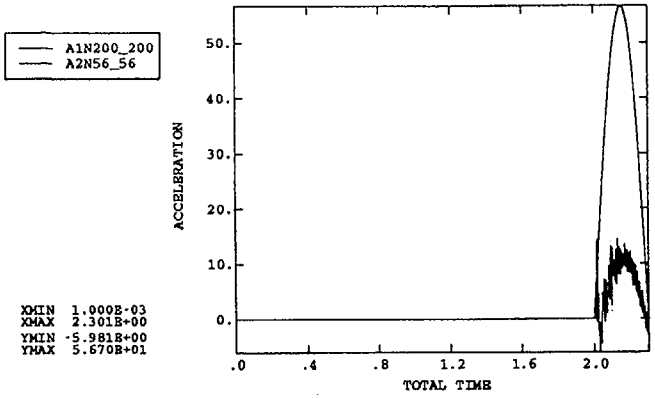

Figure 14a Applied horizontal acceleration
Vertical acceleration of corner

ABAQUS

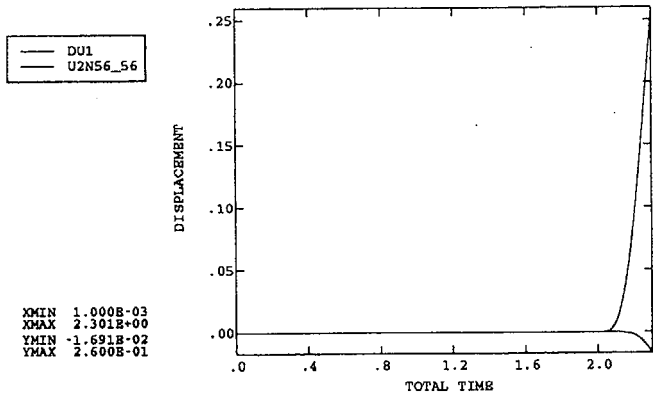

Figure 14b Vertical and horizontal
Displacement of corner

ABAQUS

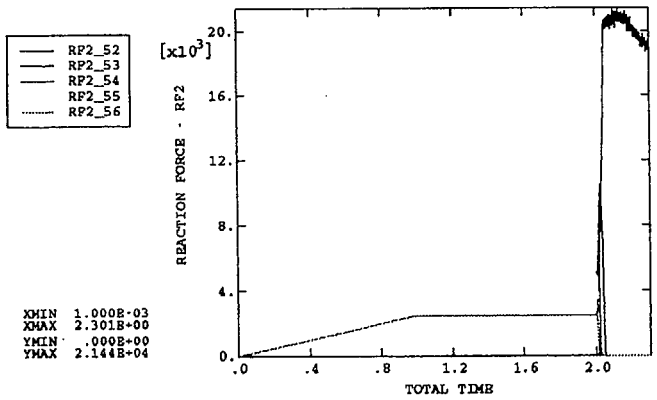

Figure 14c Reaction forces along base

ABAQUS

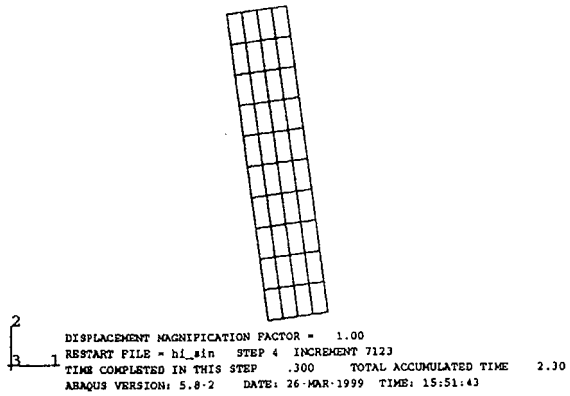

Figure 14d Displaced Block

Figure 14

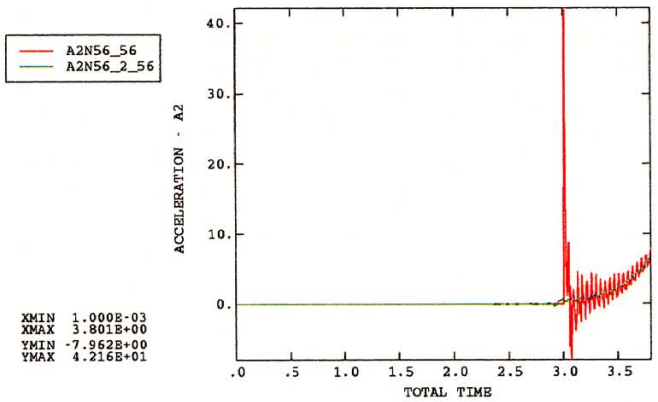

Figure 5a. Acceleration of corner node

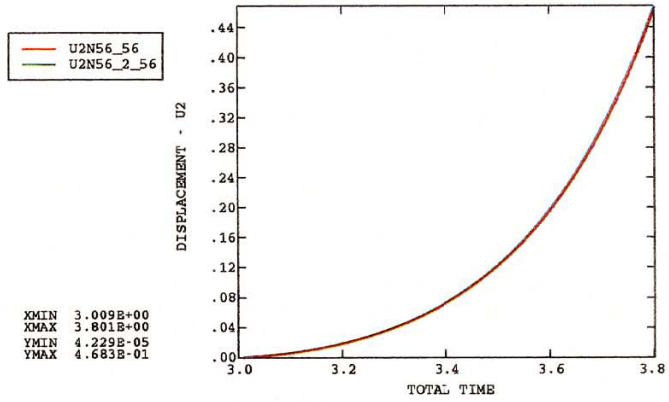

Figure 5b. Displacement of corner node

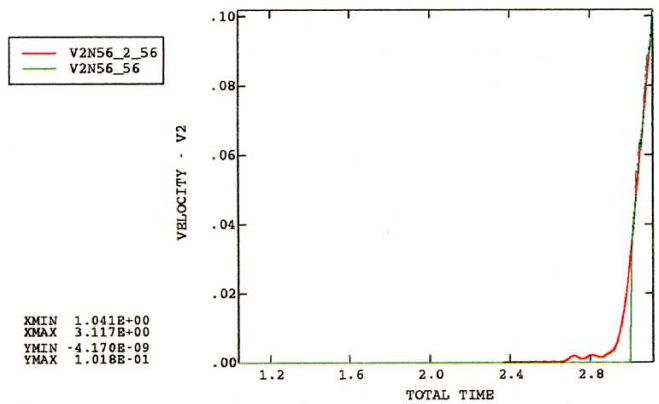

Figure 5c. Velocity of corner node

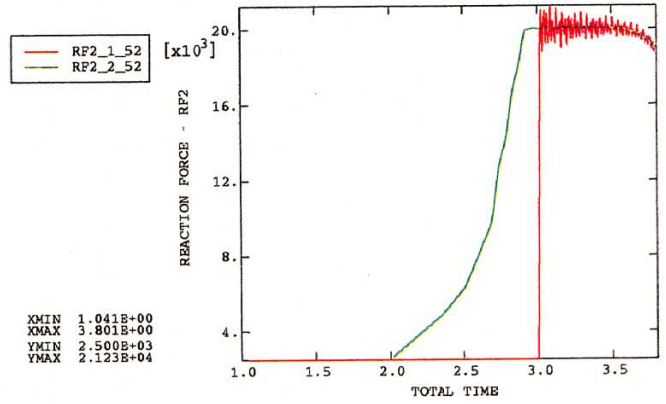

Figure 5d. Reaction force at corner node

Figure 5

ABAQUS

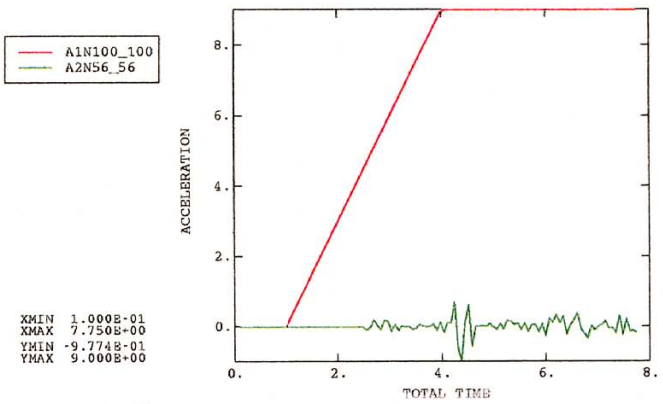

Figure 6a. Applied horizontal acceleration
Vertical acceleration of corner

ABAQUS

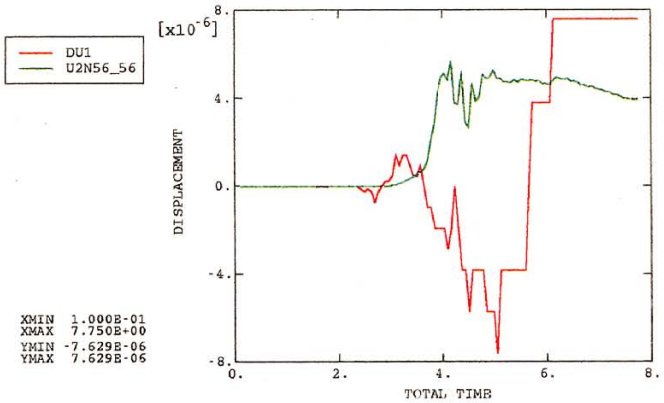

Figure 6b. Vertical and horizontal
displacement of corner

ABAQUS

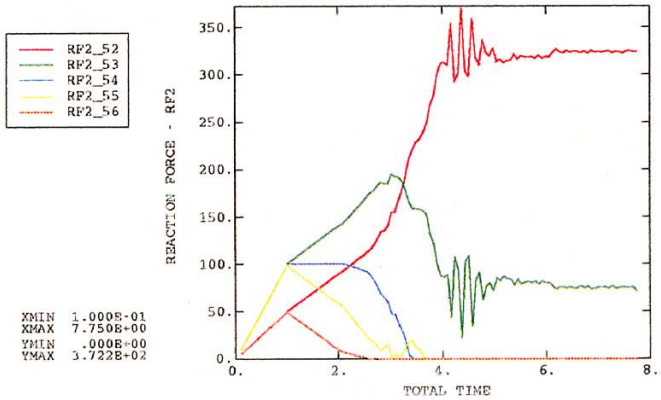

Figure 6c. Reaction forces along the base

ABAQUS

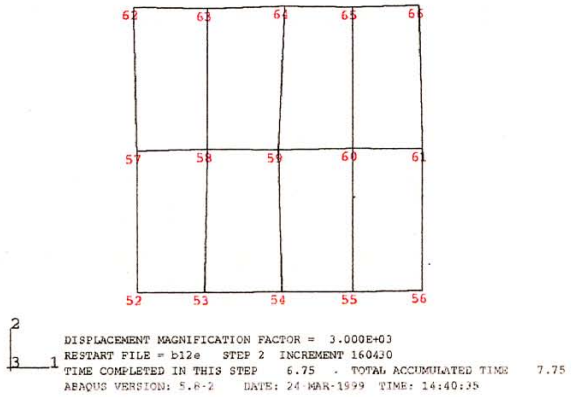

Figure 6d. Displaced block

Figure 6

ABAQUS

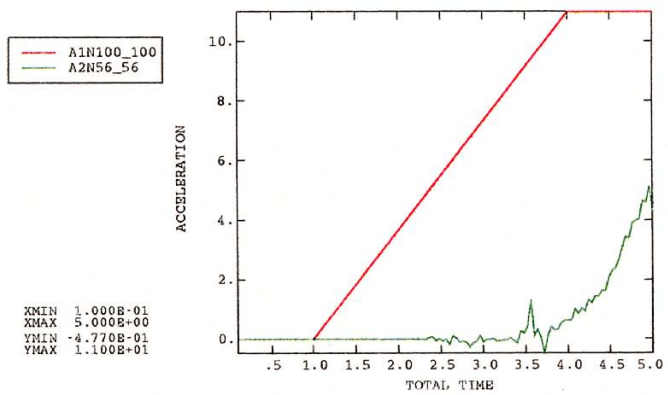

Figure 7a. Applied horizontal acceleration
Vertical acceleration of corner

ABAQUS

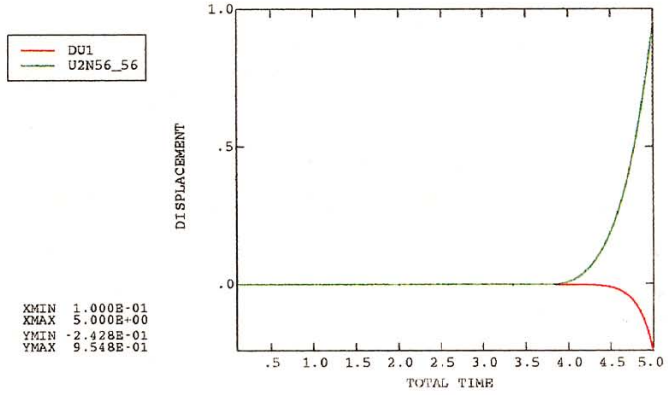

Figure 7b. Vertical and horizontal
displacement of corner

ABAQUS

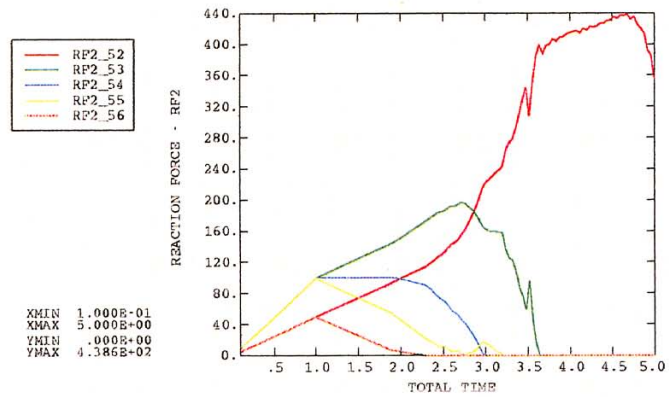

Figure 7c. Reaction forces along the base

ABAQUS

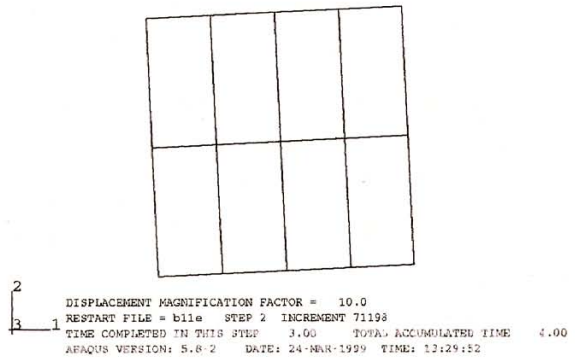

Figure 7d. Displaced block

Figure 7

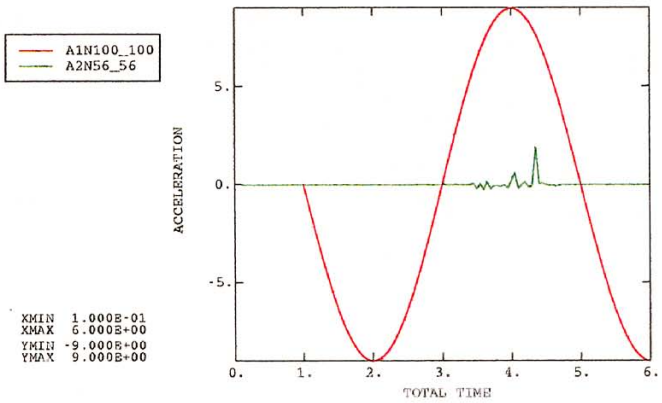

Figure 8a. Applied horizontal acceleration
Vertical acceleration of corner

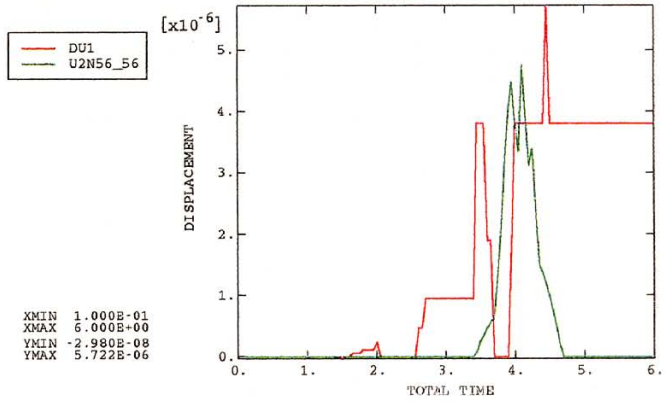

Figure 8b. Vertical and horizontal
displacement of corner

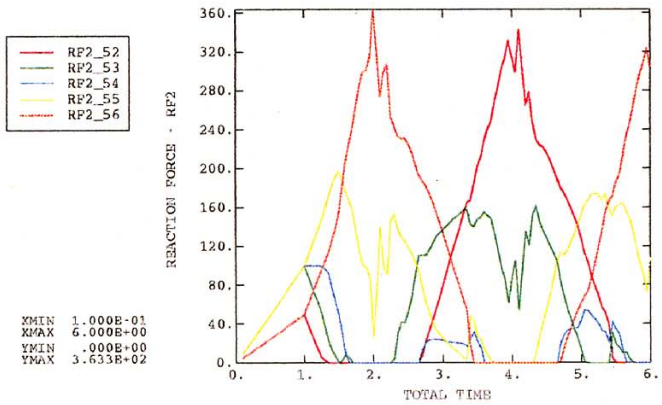

Figure 8c. Reaction forces along the base

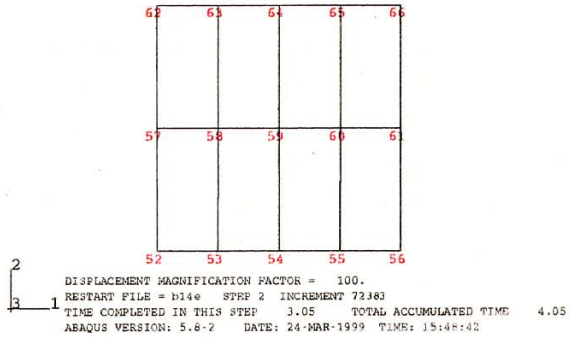

Figure 8d. Displaced block

Figure 8

ABAQUS

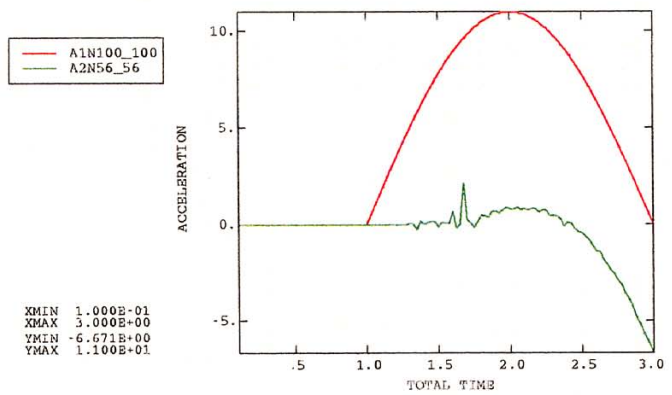

Figure 9a. Applied horizontal acceleration
Vertical acceleration of corner

ABAQUS

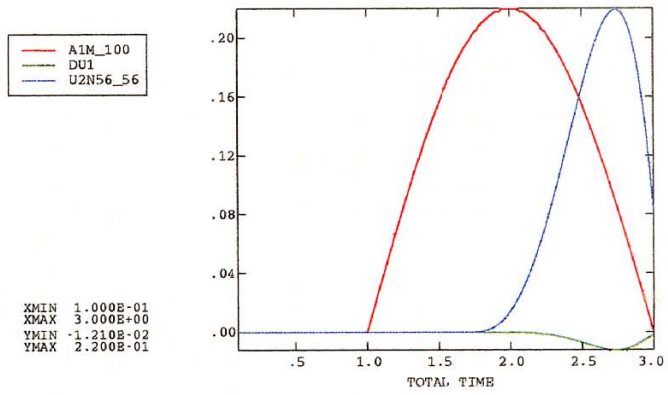

Figure 9b. Vertical and horizontal
displacement of corner

ABAQUS

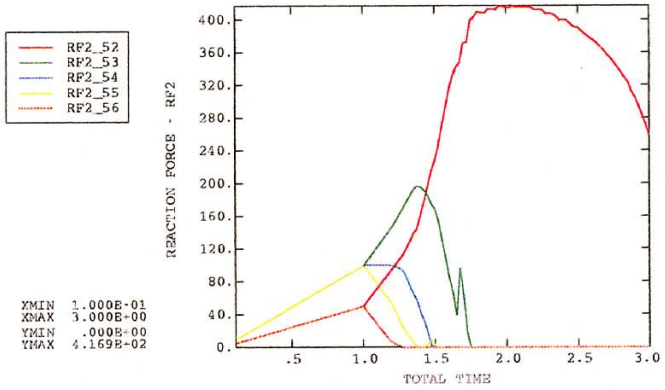

Figure 9c. Reaction forces along the base

ABAQUS

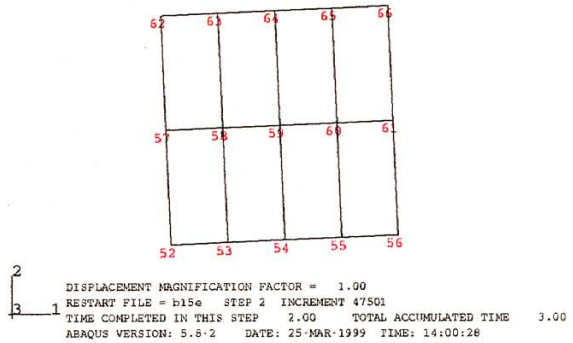

Figure 9d. Displaced block

Figure 9

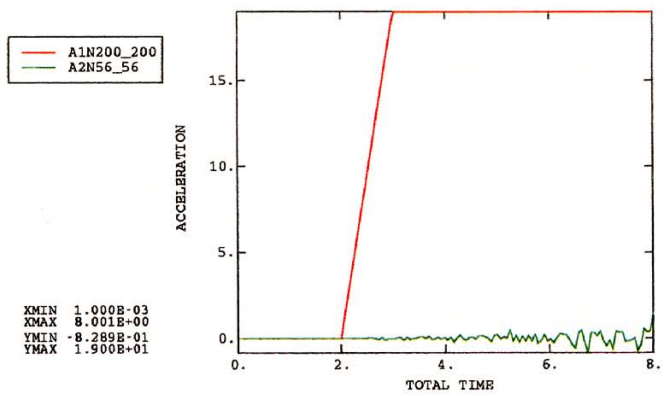

Figure 10a. Applied horizontal acceleration
Vertical acceleration of corner

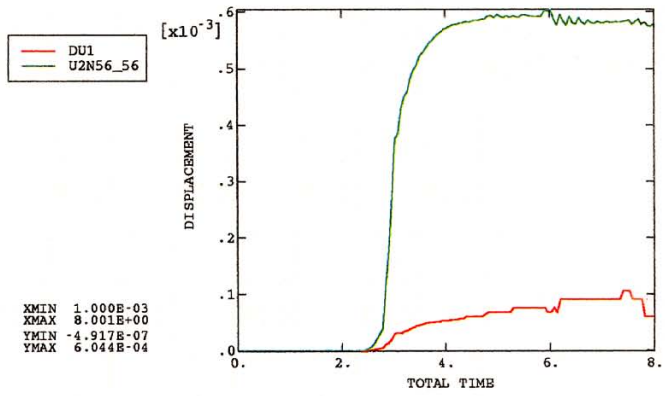

Figure 10b. Vertical and horizontal
displacement of corner

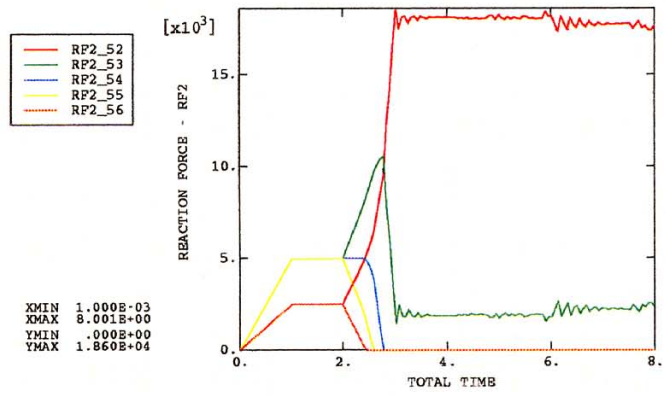

Figure 10c. Reaction forces along the base

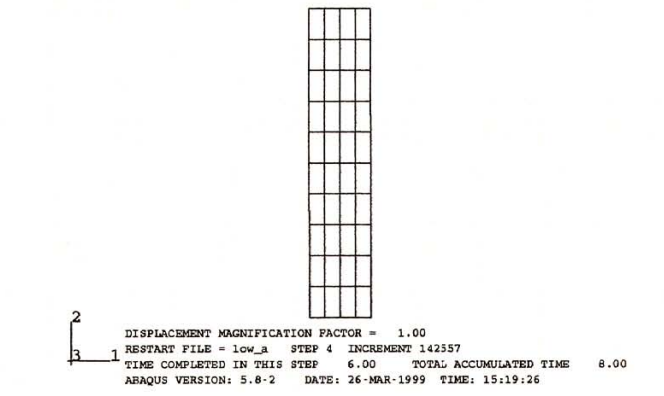

Figure 10d. Displaced block

Figure 10

ABAQUS

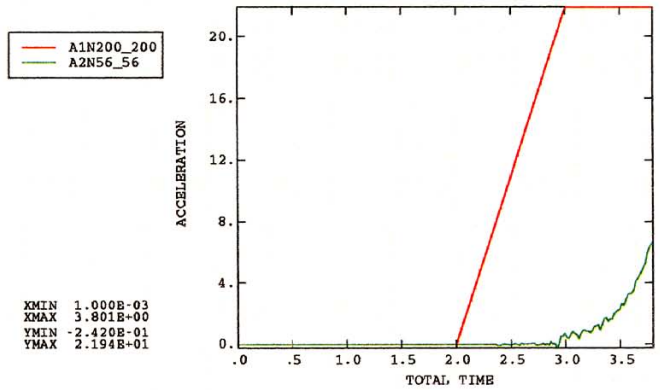

Figure 11a. Applied horizontal acceleration
Vertical acceleration of corner

ABAQUS

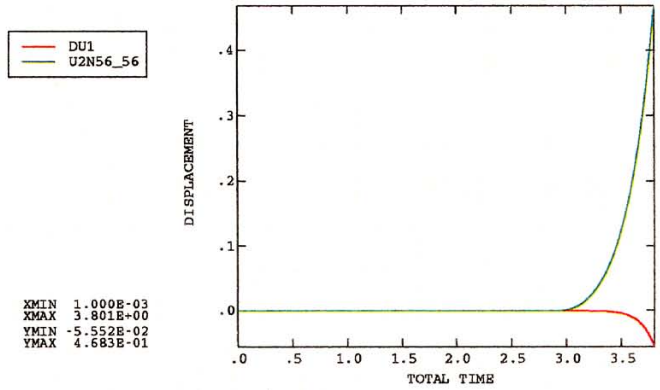

Figure 11b. Vertical and horizontal
displacement of corner

ABAQUS

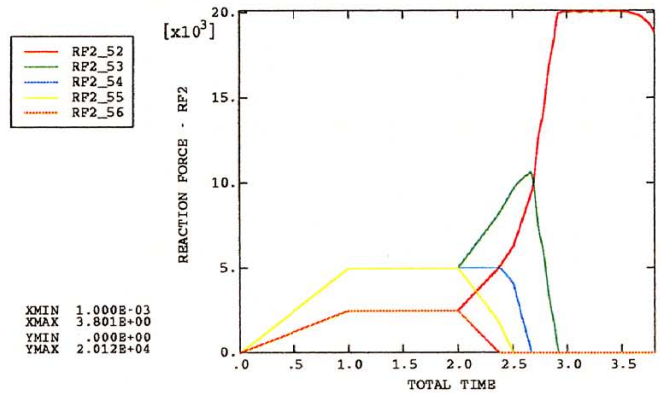

Figure 11c. Reaction forces along the base

ABAQUS

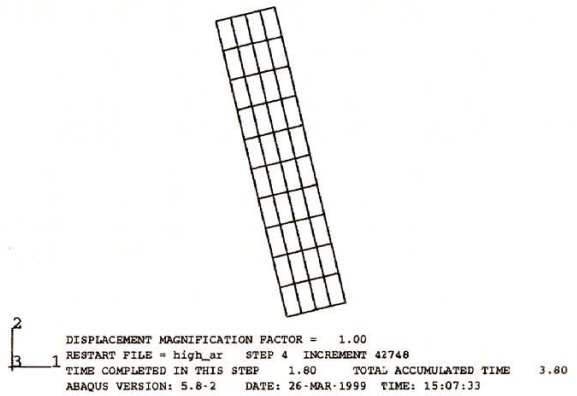

Figure 11d. Displaced block

Figure 11

ABAQUS

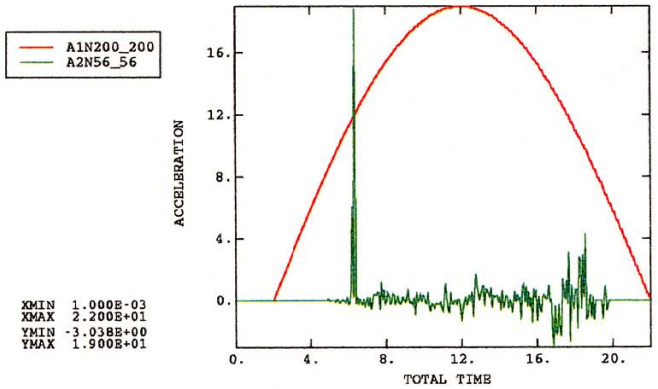

Figure 12a. Applied horizontal acceleration
Vertical acceleration of corner

ABAQUS

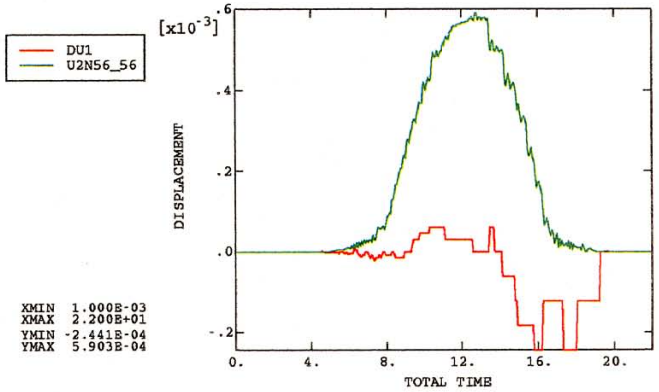

Figure 12b. Vertical and horizontal
displacement of corner

ABAQUS

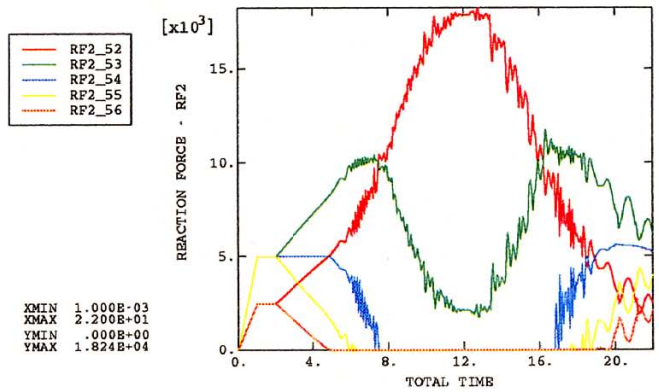

Figure 12c. Reaction forces along the base

ABAQUS

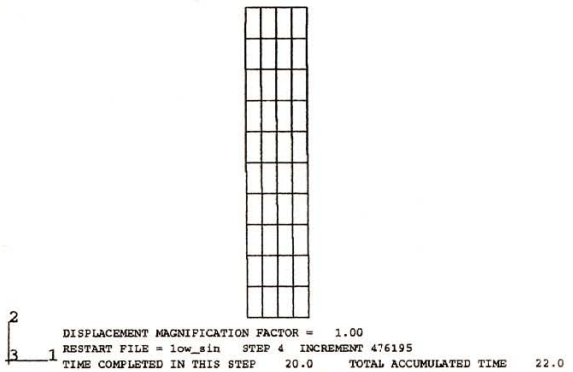

Figure 12d. Displaced block

Figure 12

ABAQUS

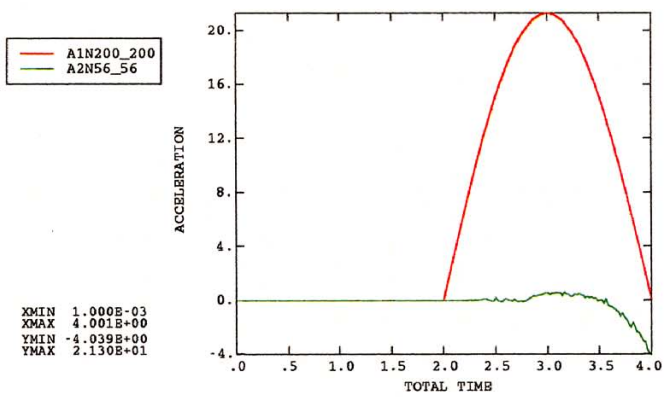

Figure 13a. Applied horizontal acceleration
Vertical acceleration of corner

ABAQUS

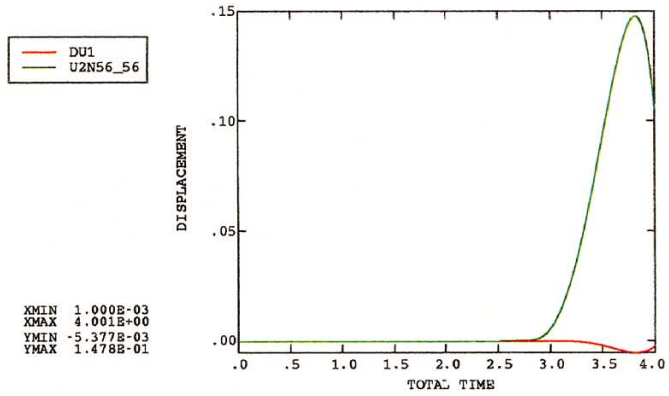

Figure 13b. Vertical and horizontal
displacement of corner

ABAQUS

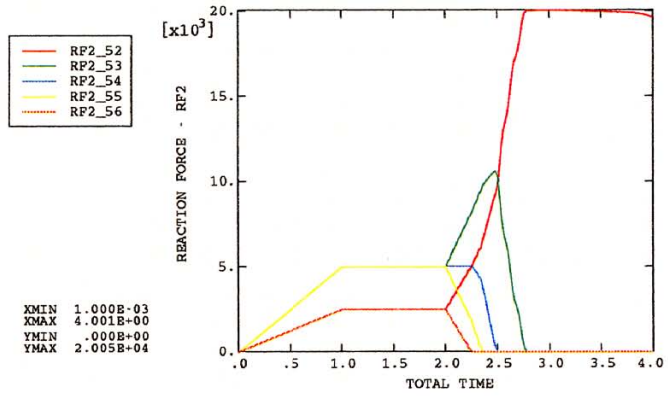

Figure 13c. Reaction forces along the base

ABAQUS

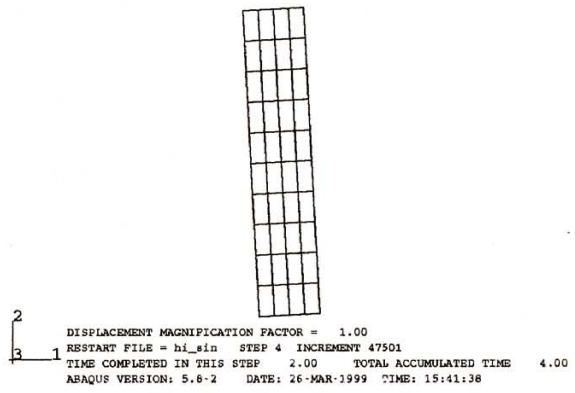

Figure 13d. Displaced block

Figure 13

ABAQUS

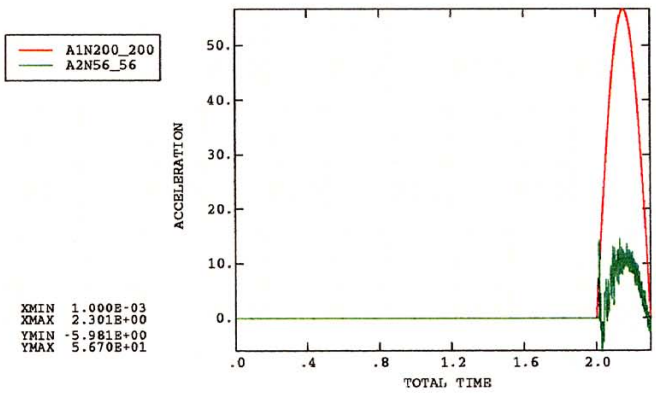

Figure 14a. Applied horizontal acceleration
Vertical acceleration of corner

ABAQUS

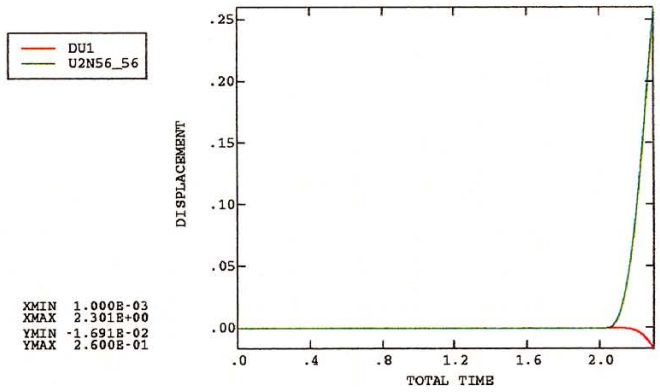

Figure 14b. Vertical and horizontal
displacement of corner

ABAQUS

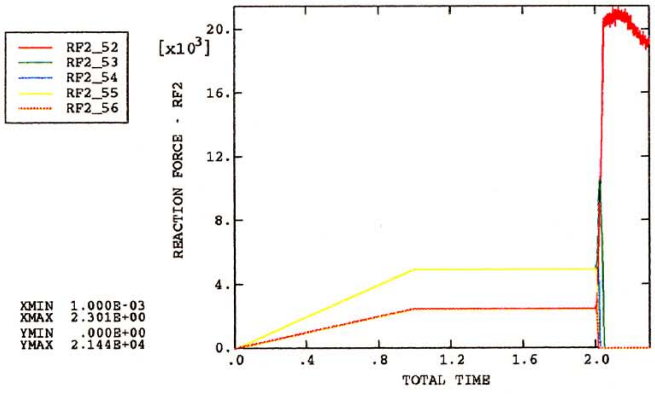

Figure 14c. Reaction forces along the base

ABAQUS

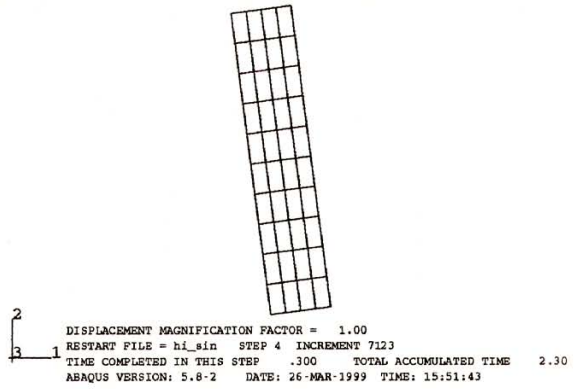

Figure 14d. Displaced block

Figure 14

Stony Gorge Ground Motions -- pvp

Velocities and Velocity Response Spectra

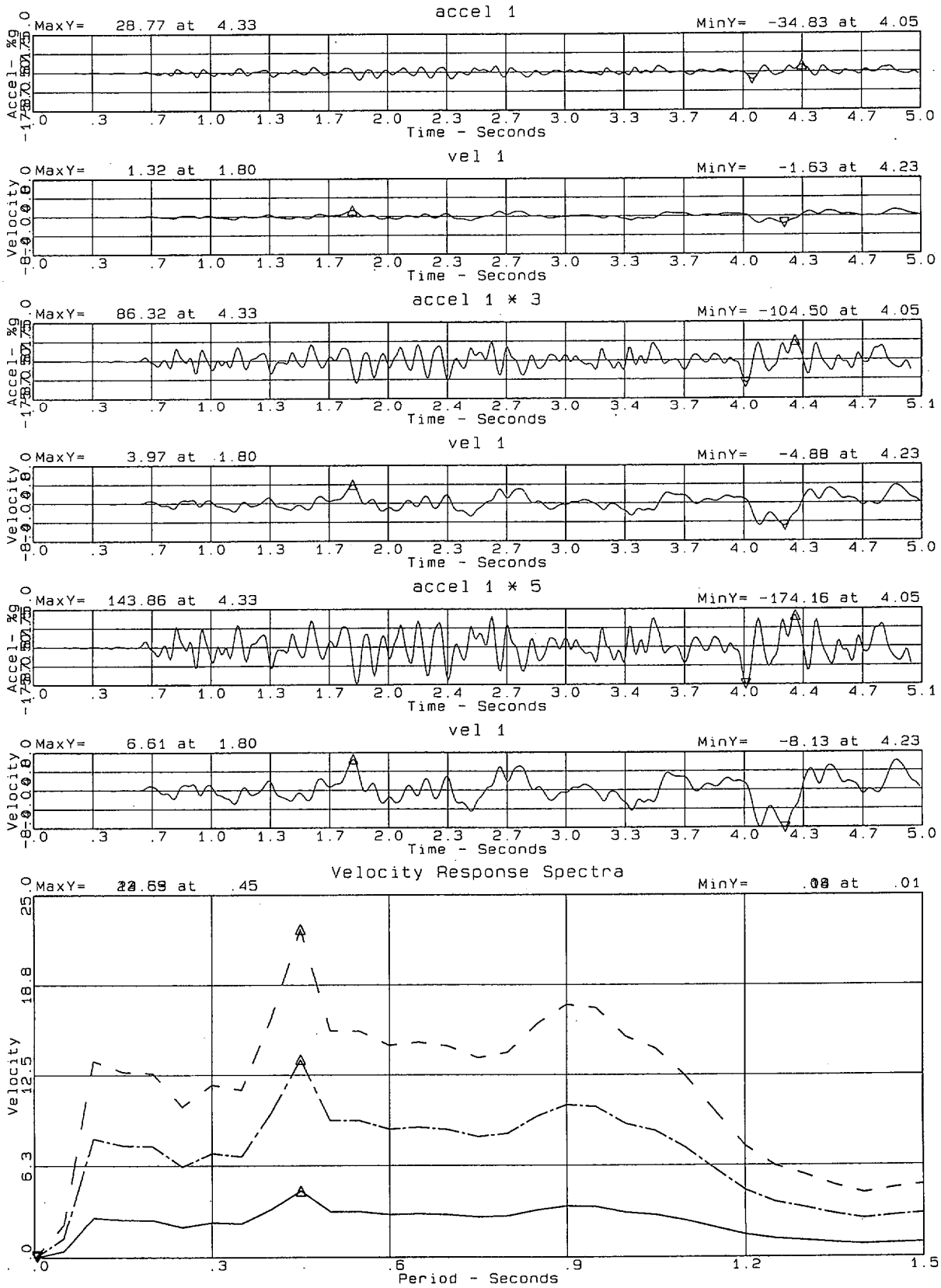

Input=integrate.p2p, Created 26-May-99 10:23:51

Figure 15

ABAQUS

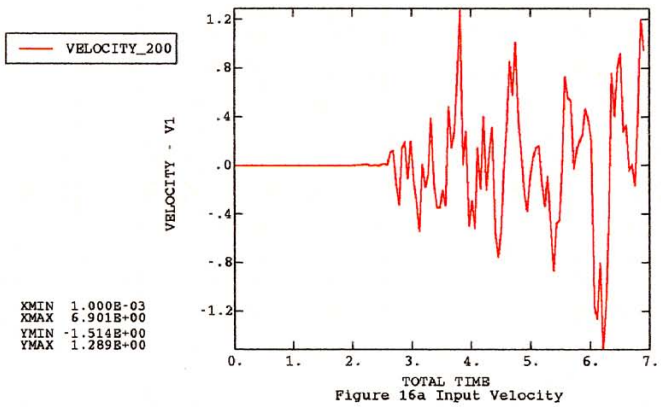

Figure 16a Input Velocity

ABAQUS

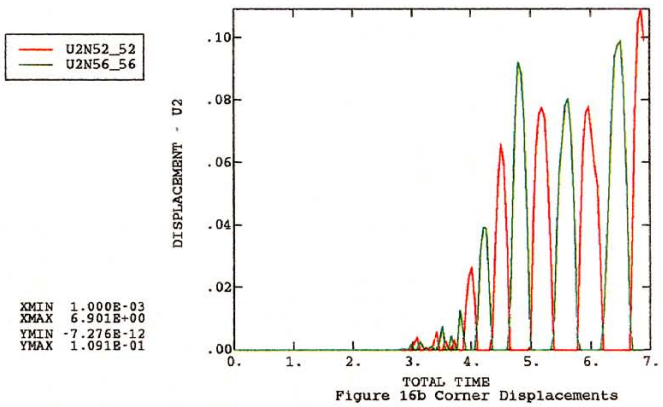

Figure 16b Corner Displacements

ABAQUS

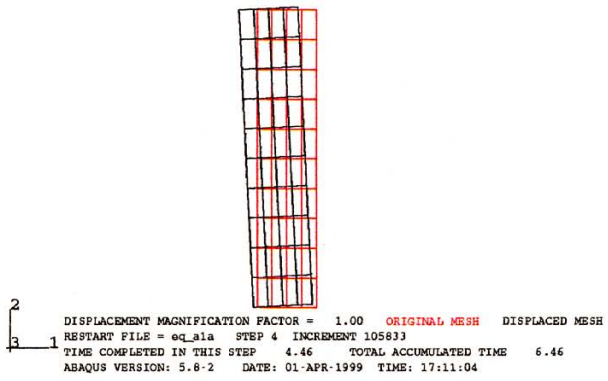

ABAQUS

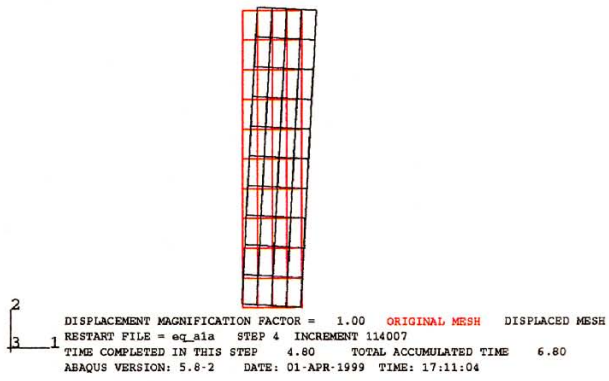

Figure 16

ABAQUS

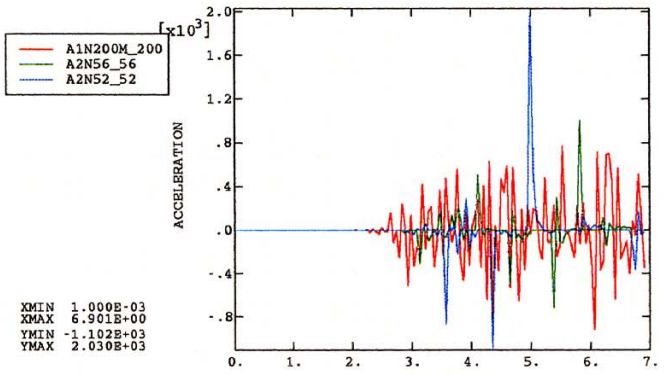

Figure 16e Input Acceleration
Corner Accelerations

ABAQUS

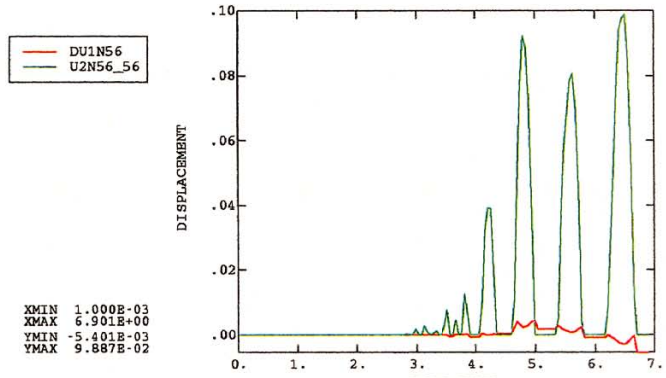

Figure 16f Horz Displacement -- corner
Vert Displacement -- corner

ABAQUS

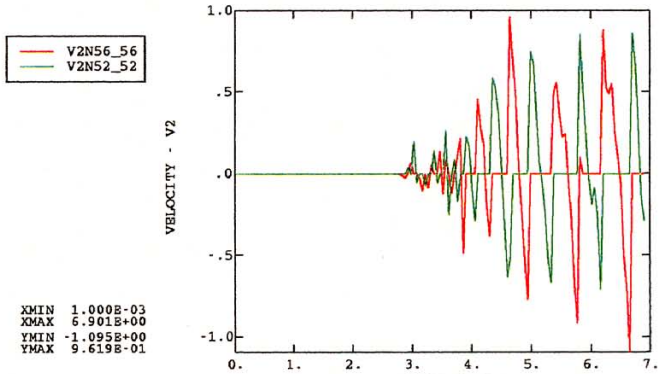

Figure 16g Vert Velocity -- corners

ABAQUS

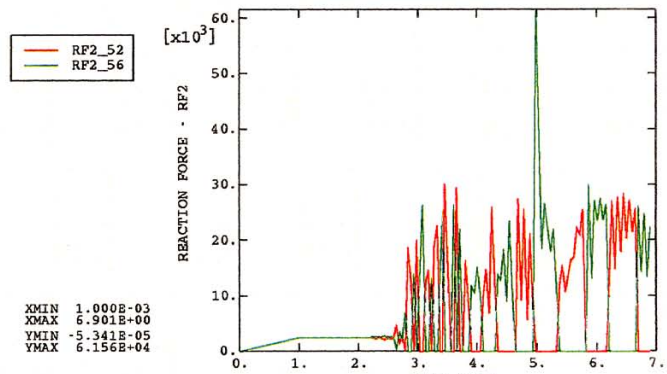

Figure 16 h Reactions at corners

Figure 16 (continued)

ABAQUS

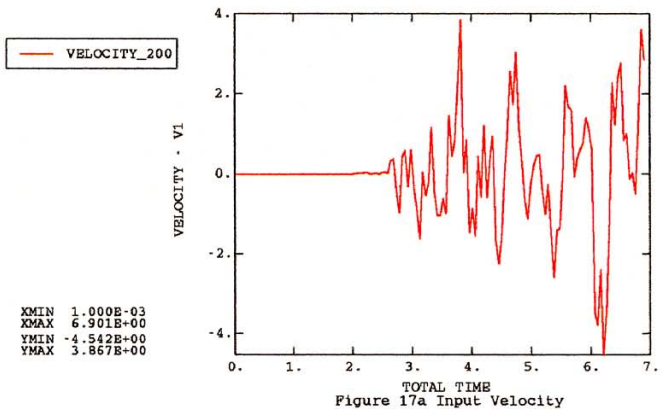

Figure 17a Input Velocity

ABAQUS

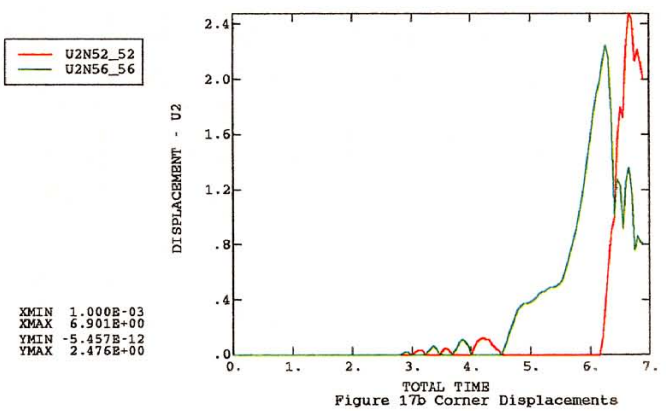

Figure 17b Corner Displacements

ABAQUS

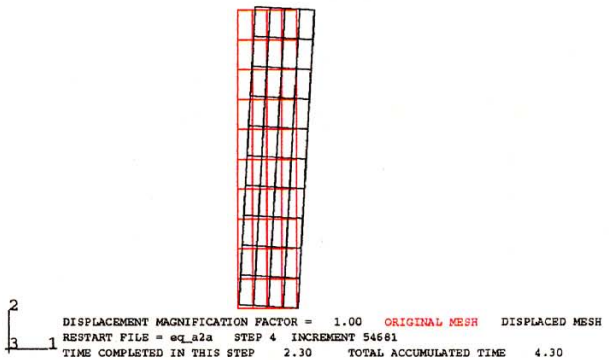

ABAQUS

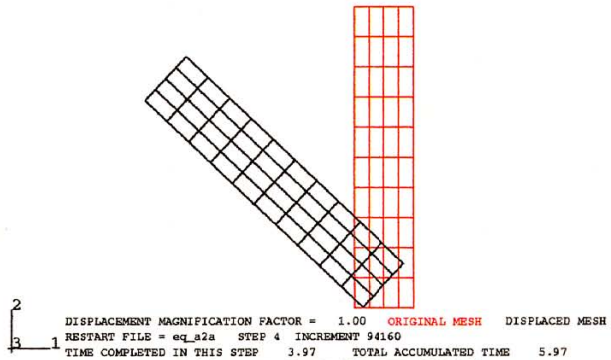

Figure 17

ABAQUS

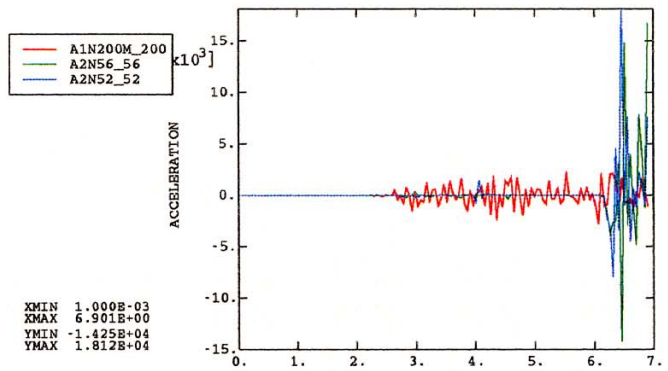

Figure 17e Input Acceleration
Corner Accelerations

ABAQUS

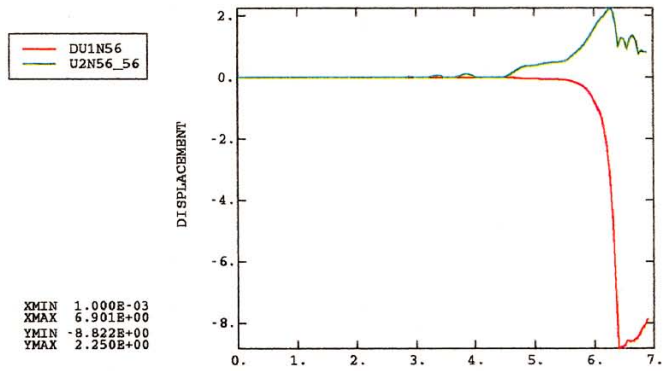

Figure 17f Horz Displacement -- corner
Vert Displacement -- corner

ABAQUS

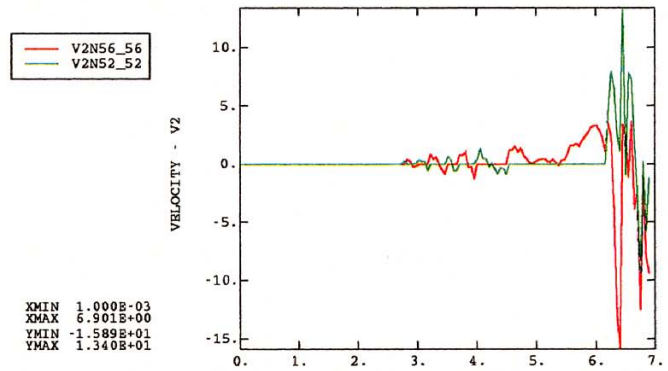

Figure 17g Vert Velocity -- corners

ABAQUS

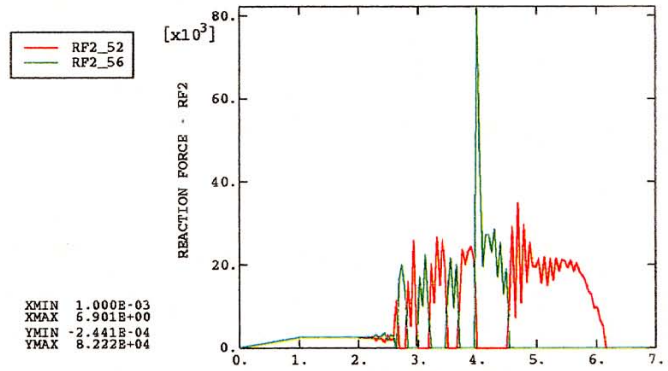

Figure 17 h Reactions at corners

Figure 17 (continued)

ABAQUS

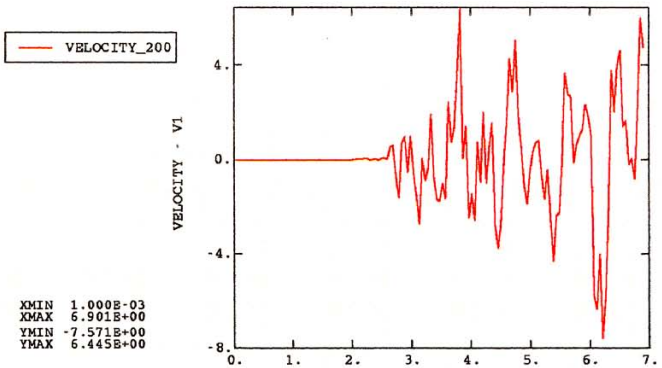

Figure 18a Input Velocity

ABAQUS

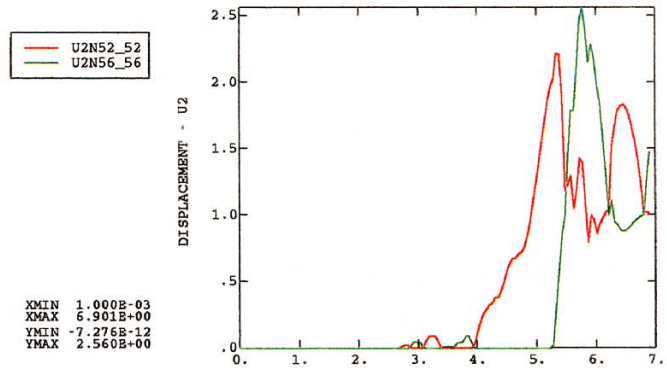

Figure 18b Corner Displacements

ABAQUS

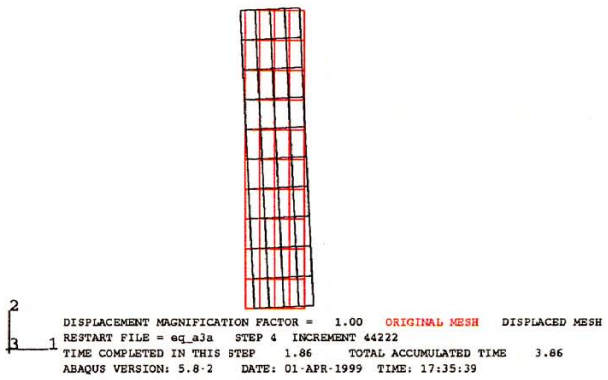

ABAQUS

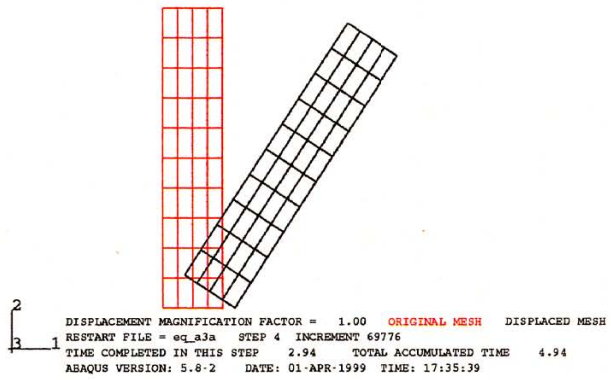

Figure 18

ABAQUS

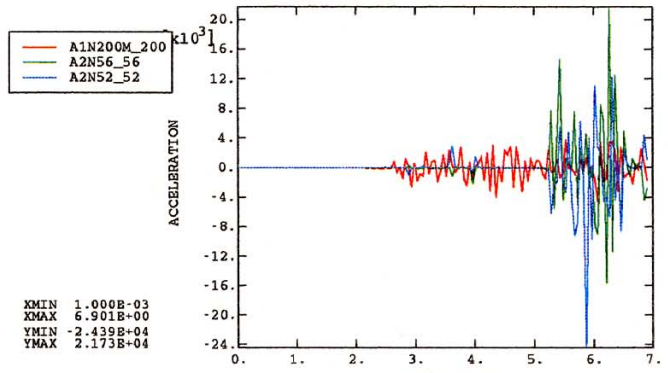

Figure 18e Input Acceleration
Corner Accelerations

ABAQUS

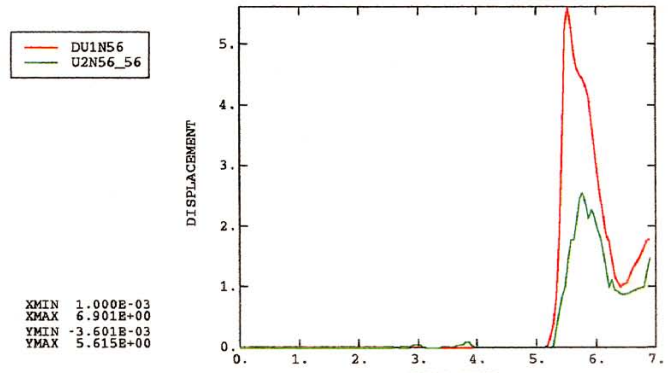

Figure 18f Horz Displacement -- corner
Vert Displacement -- corner

ABAQUS

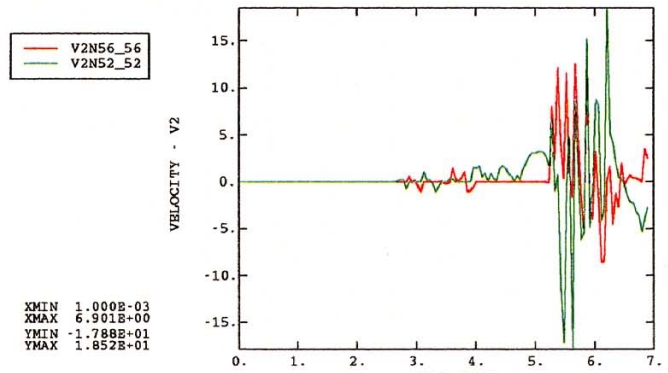

Figure 18g Vert Velocity -- corners

ABAQUS

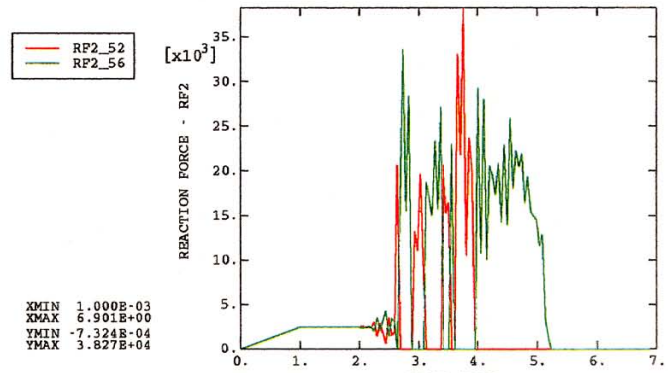

Figure 18 h Reactions at corners

Figure 18 (continued)

Hoover Model

Ground Motions and Velocity Response spectra

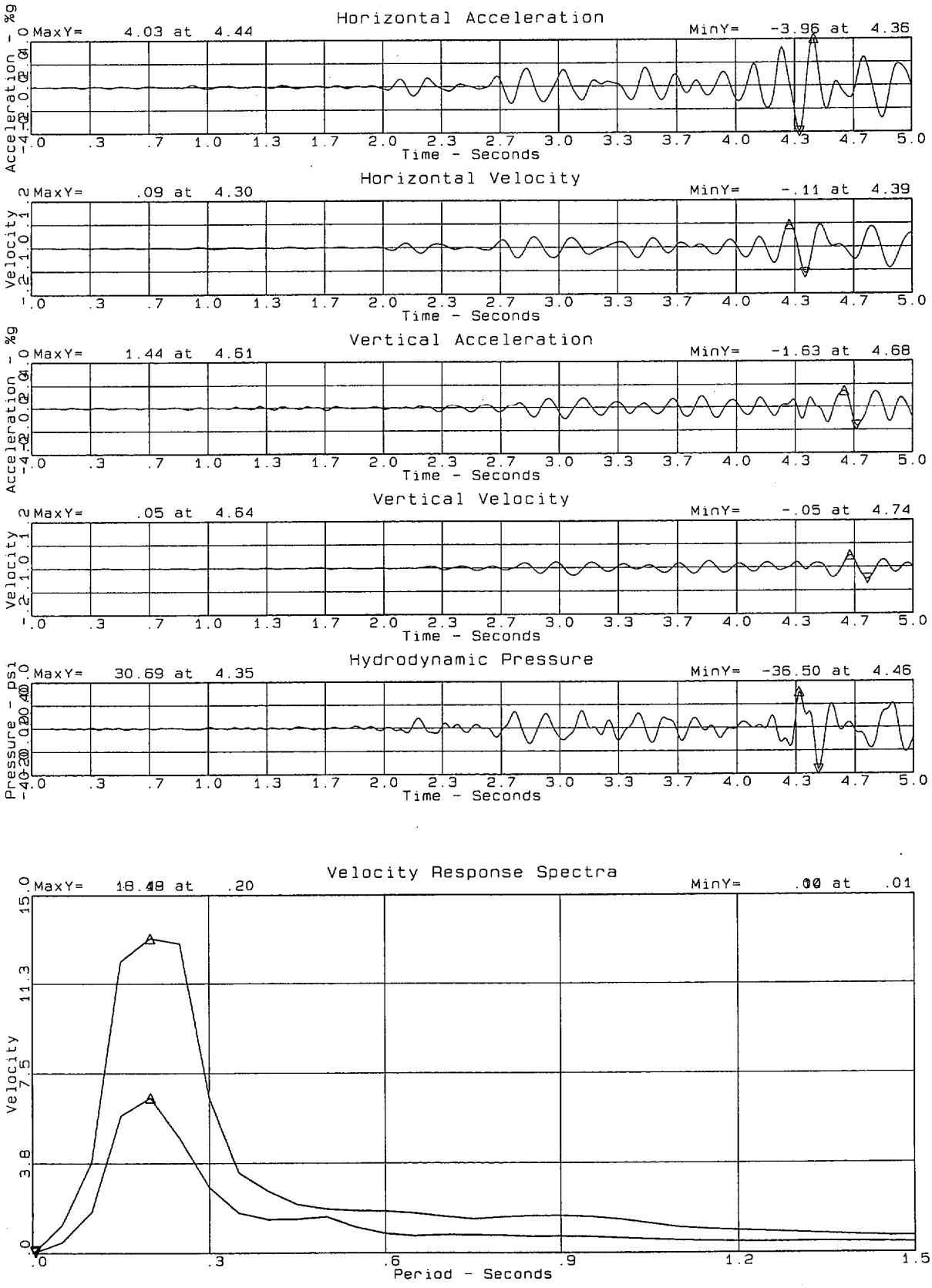

Input=eq_press.p2p, Created 23-Jun-99 09:54:54

Figure 19

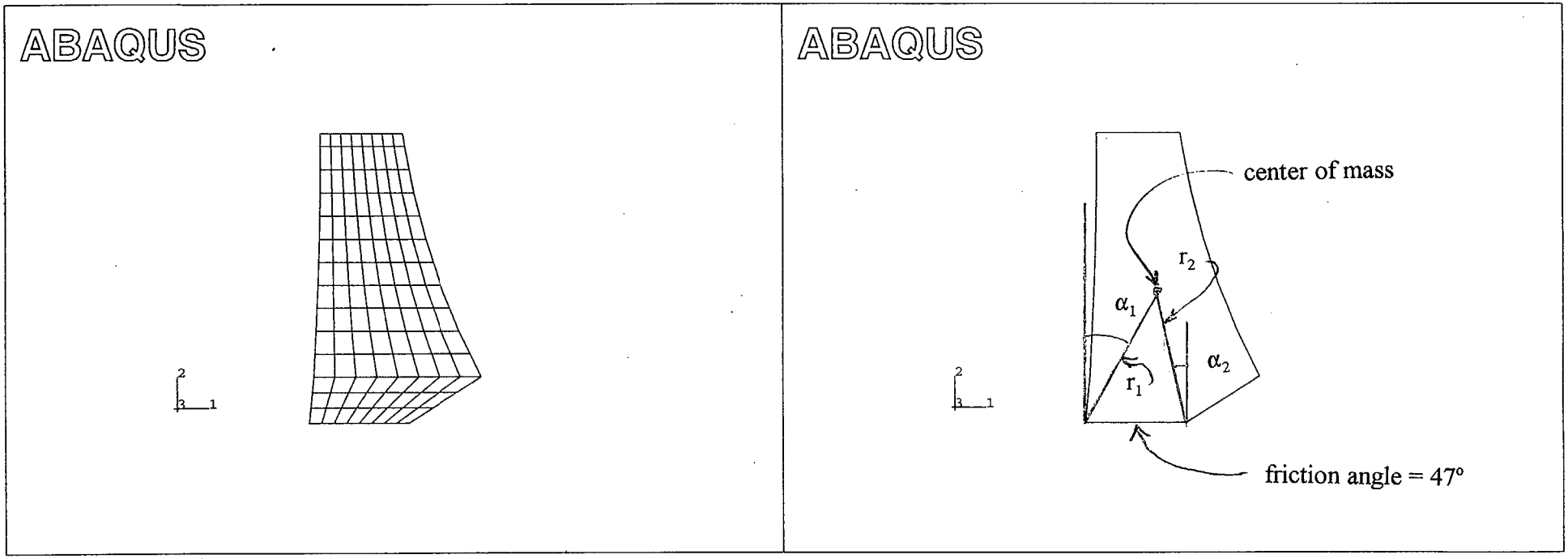

Figure 20 -- Finite Element Model of a Postulated Block at the Top of Hoover Dam

ABAQUS

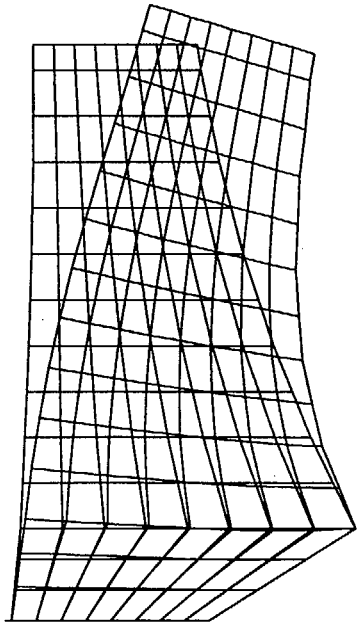

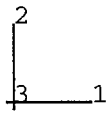

DISPLACEMENT MAGNIFICATION FACTOR = 385. ORIGINAL MESH DISPLACED MESH
RESTART FILE = hvr_mode STEP 1 INCREMENT 1
EIGENMODE 1 FREQUENCY = 6.20 (CYCLES/TIME)
ABAQUS VERSION: 5.8-2 DATE: 02-APR-1999 TIME: 12:33:33

Figure 21

ABAQUS

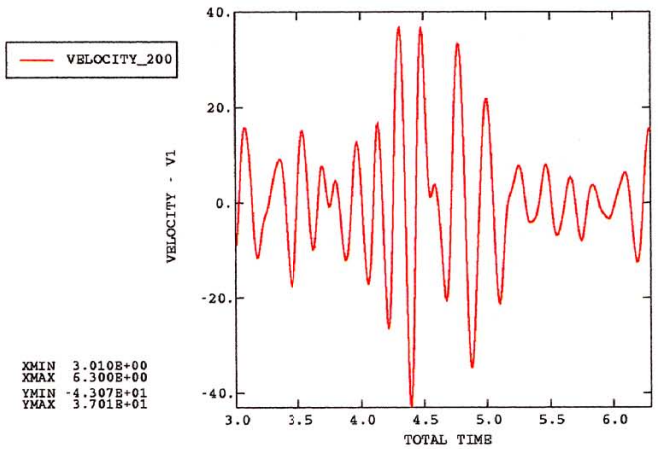

Figure 23a Input Velocity

ABAQUS

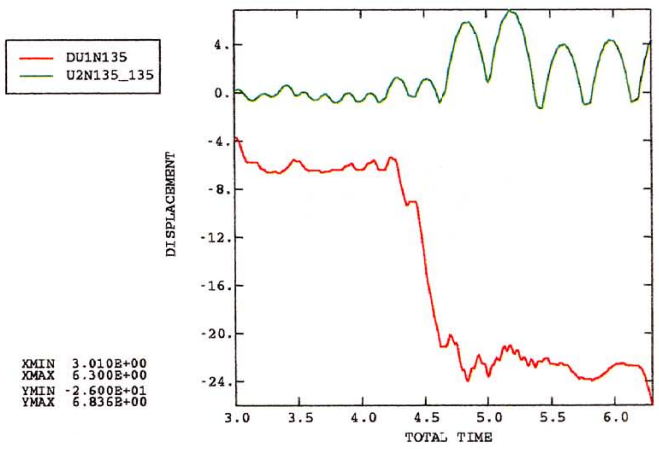

Figure 23b Horz Displacement -- corner
Vert Displacement -- corner

ABAQUS

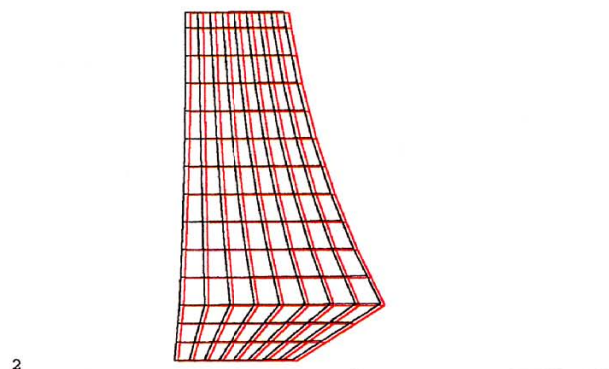

Figure 23c

ABAQUS

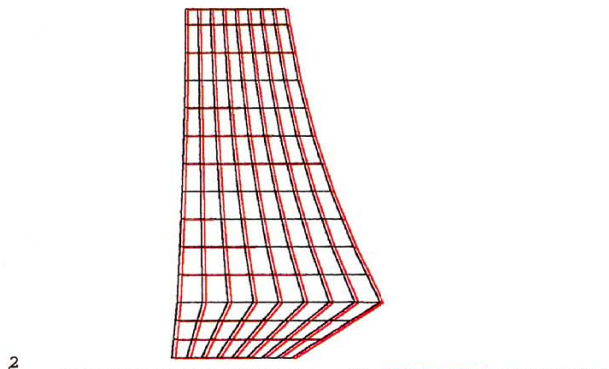

Figure 23d

Figure 22

ABAQUS

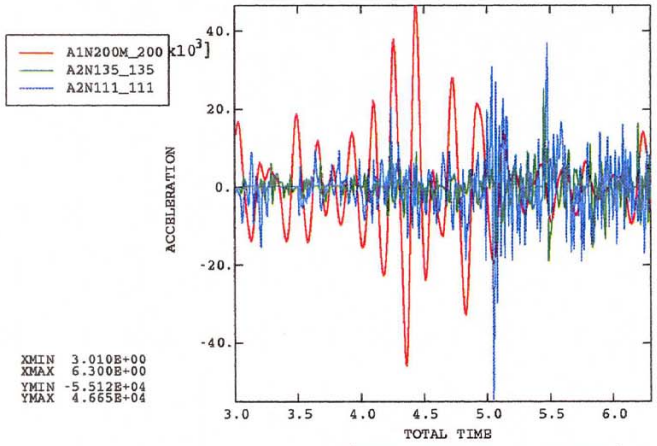

Figure 23e Input Acceleration
Corner Accelerations

ABAQUS

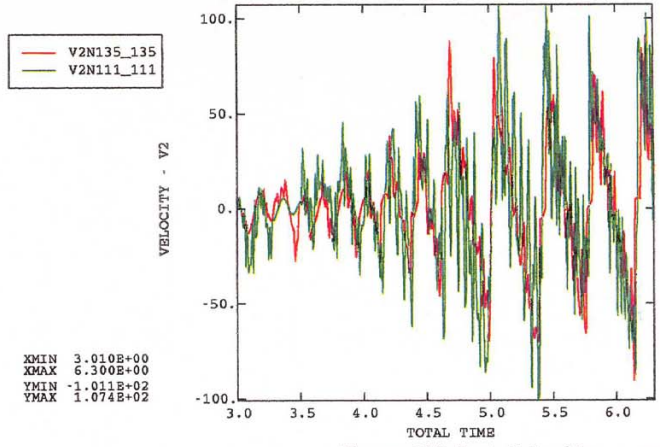

Figure 23f Vert Velocity -- corners

ABAQUS

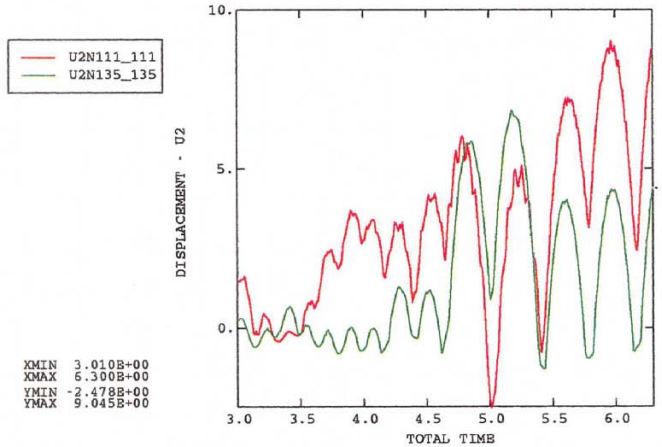

Figure 23g Corner Displacements

ABAQUS

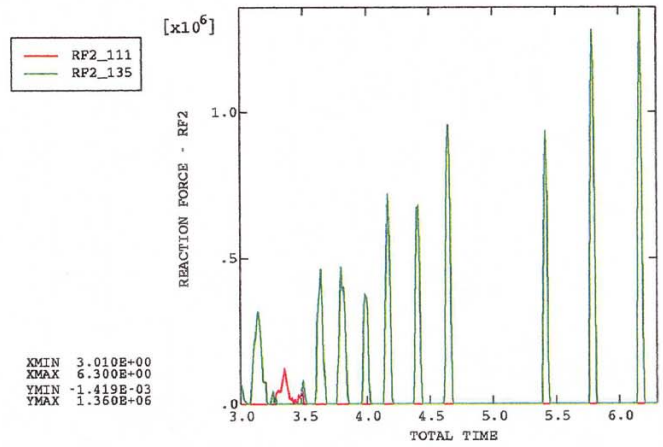

Figure 23h Reactions at corners

Figure 22 (Continued)